ELECTROMAGNETIC SCATTERING FROM CLUSTER OF SPHERES USING DIAGONALIZED VECTOR ADDITION THEOREM

A THESIS SUBMITTED TO
THE GRADUATE SCHOOL OF NATURAL AND APPLIED SCIENCES
OF
MIDDLE EAST TECHNICAL UNIVERSITY

BY

HALİL İBRAHİM ATASOY

IN PARTIAL FULFILLMENT OF THE REQUIREMENTS
FOR
THE DEGREE OF DOCTOR OF PHILOSOPHY
IN
ELECTRICAL AND ELECTRONICS ENGINEERING

SEPTEMBER 2014

SEPTEMBER 2014

Approval of the thesis:

ELECTROMAGNETIC SCATTERING FROM CLUSTER OF SPHERES USING DIAGONALIZED VECTOR ADDITION THEOREM

submitted by **HALİL İBRAHİM ATASOY** in partial fulfillment of the requirements for the degree of **Doctor of Philosophy in Electrical and Electronics Engineering Department, Middle East Technical University** by,

Prof. Dr. Canan ÖZGEN _____
Dean, Graduate School of **Natural and Applied Sciences**

Prof. Dr. Gönül TURHAN SAYAN _____
Head of Department, **Electrical and Electronics Eng.**

Prof. Dr. Sencer KOÇ _____
Supervisor, **Electrical and Electronics Eng. Dept., METU**

Examining Committee Members :

Prof. Dr. Özlem AYDIN ÇİVİ _____
Electrical and Electronics Engineering Dept., METU

Prof. Dr. Sencer KOÇ _____
Electrical and Electronics Engineering Dept., METU

Prof. Dr. Mustafa KUZUOĞLU _____
Electrical and Electronics Engineering Dept., METU

Asst. Prof. Dr. Özgür ERGÜL _____
Electrical and Electronics Engineering Dept., METU

Prof. Dr. Ayhan ALTINTAŞ _____
Electrical and Electronics Eng. Dept., Bilkent University

Date: 26.09.2014

I hereby declare that all information in this document has been obtained and presented in accordance with academic rules and ethical conduct. I also declare that, as required by these rules and conduct, I have fully cited and referenced all material and results that are not original to this work.

Name, Last name : Halil İbrahim ATASOY

Signature :

ABSTRACT

ELECTROMAGNETIC SCATTERING FROM CLUSTER OF SPHERES USING DIAGONALIZED VECTOR ADDITION THEOREM

ATASOY, Halil İbrahim

Ph.D., Department of Electrical and Electronics Engineering

Supervisor: Prof. Dr. S. Sencer KOÇ

September 2014, 83 pages

Our aim is to implement an FMM (Fast Multipole Method) solver using the approach given by Chew [35] for diagonalization of vector addition theorem. Scatterer bodies will be modeled as ensemble of smaller spheres with same constitutive properties and then will be analyzed using the FMM solver.

For general scattering problems, it is hard to obtain an analytical solution. There are only some special cases where exact solutions are possible. Hence, for the investigation of problems where numbers of scatterers are high, numerical methods like FMM are necessary. For the analysis of scattering problem, FMM is an effective tool. Hence, mathematical background of the method is investigated. Addition theorem is examined for the expression of the wave functions in distinct coordinate systems. Starting from the scalar addition theorem, vector addition theorem in spherical coordinates is investigated. Since, computation period spent for the calculation of the translation coefficients is high; recursive methods for the calculations are also analyzed.

Keywords: Scattering, Fast Multipole Method, Addition Theorems, BiCGSTAB

ÖZ

VEKTÖR TOPLAMA YÖNTEMİNİN KÖŞEGENLEŞTİRİLMESİ İLE KÜRE KÜMESİNDEN ELEKTROMANYETİK YANSIMA HESAPLANMASI

ATASOY, Halil İbrahim
Doktora, Elektrik ve Elektronik Mühendisliği Bölümü
Tez Yöneticisi: Prof. Dr. S. Sencer KOÇ

Eylül 2014, 83 sayfa

Bu çalışmadaki amacımız, Chew'ın [35] gösterdiği vektör toplam yönteminin köşegenleştirilmesini uygulayarak HÇKY(Hızlı Çok Kutuplama Yöntemi) çözücüsünün gerçekleştirilmesidir. Yansıtıcı cisimler aynı özelliklerde daha küçük kürelerin birleşimi olarak modellenip HÇKY çözücüsü ile analiz edilecektir.

Genel saçınım problemlerinde analitik çözüme ulaşmak sadece birkaç özel durum için mümkün olmaktadır. Bu nedenle yansıtıcı cisim sayısının yüksek olduğu durumlarda HÇKY benzeri nümerik yöntemlerin kullanımı gerekli olmaktadır. Saçınım problemlerinin çözümünde HÇKY yöntemi etkili bir yöntemdir. Bu nedenle bu metodun matematiksel altyapısı incelenmiştir. Dalga fonksiyonlarının farklı koordinat düzlemlerinde ifade edilmesini sağlamak için toplama teoremi incelenmiştir. Yönsüz toplam yöntemi ile başlanıp, küresel koordinat düzleminde yönlü toplama teoremi incelenmiştir. Dalga fonksiyonlarının farklı koordinatlara ötelenmesi için kullanılan katsayıların hesabı uzun sürdüğünden, tekrarlamalı yöntemler de incelenmiştir.

Anahtar kelimeler: Elektromanyetik Saçınım, Hızlı Çok Kutuplama Yöntemi, Toplam Teoremi, BiCGSTAB.

To My Family

ACKNOWLEDGEMENTS

I would like to thank Prof. Dr. S. Sencer KOÇ for valuable supervision, guidance and motivation of this thesis for years.

I would like to thank to Prof. Dr. Özlem AYDIN ÇİVİ for providing valuable suggestions for years.

I would like to thank to Asst. Prof. Dr. Özgür ERGÜL for providing valuable suggestions on FMM and simulation results.

I would like to thank to Prof. Dr. Mustafa KUZUOĞLU and Prof. Dr. Ayhan ALTINTAŞ for guidance and participating in the thesis defence jury.

I would also to thank İrem ATASOY for her support and motivation.

I would like express my gratitude towards my family for their support throughout this study and I want to dedicate this work to my parents.

TABLE OF CONTENTS

ABSTRACT v

ÖZ vi

ACKNOWLEDGEMENTS viii

TABLE OF CONTENTS ix

LIST OF TABLES xi

LIST OF FIGURES xii

LIST OF ABBREVIATIONS xvii

CHAPTERS

1. INTRODUCTION 1
   - 1.1 Background and Scope 1
   - 1.2 Advantages of the Fast Multipole Method 5
   - 1.3 Diagonalization of Translation Operators in FMM 5
   - 1.4 Organization of the Thesis 6
2. VECTOR SPHERICAL WAVE FUNCTIONS, SCALAR AND VECTOR ADDITION THEOREM 7
   - 2.1 Introduction 7
   - 2.2 Vector Spherical Wave Functions 7
   - 2.3 Scalar and Vector Translational Addition Theorems 12
   - 2.4 Recurrence Relations for Vector Addition Theorem 15
     - 2.4.1 Multipole Expansion of a Plane Wave 21
3. T-MATRIX FORMULATION 23
   - 3.1 Introduction 23
   - 3.2 Surface Integral Equations 24

3.2.1 Surface Integral Equations for the Electromagnetic Problems 24
3.3 Extended Boundary Condition Method 28
3.4 T-matrix Formulation 29
3.4.1 T-Matrix Coefficients 32
3.4.2 Iterative Methods 34
4. DIAGONALIZATION OF THE VECTOR ADDITION THEOREM 37
4.1 Introduction 37
4.2 Diagonalization of the Spherical Translation Operators 41
4.3 Diagonalization of Vector Addition Theorem 42
4.3.1 An Orthogonality Identity 44
4.3.2 Diagonalization 45
4.4 Error Sources 46
4.5 Numerical Results 50
4.5.1 Scattering Calculations of Dielectric Bodies 51
4.5.2 Scattering Calculations of NASA Almond 61
5. CONCLUSIONS 73
REFERENCES 75
CURRICULUM VITAE 83

LIST OF TABLES

TABLES

Table 4-1 Performance parameters for dielectric scattering problems for 0.1-0.3λ 60

Table 4-2 Performance parameters for dielectric scattering problems for 0.35-0.55λ 60

Table 4-3 Performance parameters for dielectric scattering problems for 0.6-0.75λ 61

LIST OF FIGURES

Figure 2.1 Vector representation of **M** fields. (From top to bottom $\mathbf{M}_{10}$, $\mathbf{M}_{20}$, $\mathbf{M}_{30}$ are shown) 9
Figure 2.2 Vector representation of **N** fields. From top to bottom $\mathbf{N}_{10}$, $\mathbf{N}_{20}$, $\mathbf{N}_{30}$ are shown) 10
Figure 2.3 Vector representation of $\mathbf{M}_{11}$ field. 10
Figure 2.4 Vector representation of $\mathbf{N}_{11}$ field. 11
Figure 2.5 Translation of the coordinate axes to new coordinate frame located at r, θ, ϕ. 13
Figure 3.6 Translation coefficient calculation for increasing n and m. Translation coefficients along the diagonal shown in figure with vector R_1 is calculated using the initial values $\beta\nu\mu, 00$ and recursion formulas (2-45) and (2-46). 20
Figure 3.7 Translation coefficient calculation for increasing n and m. Translation coefficients along the diagonal shown in figure with vector R_2 is calculated using the initial values $\beta\nu\mu, 00$ and recursion formulas (2-55) and (2-56). 20
Figure 2.8 Translation coefficient calculations for increasing n and constant m. Column vector shown in figure with vector R_3 is calculated by the recursion formulas (2-50) and (2-51) with the use of the initial values along the diagonal vectors R_1 and R_2. 21
Figure 3.1 Electromagnetic scattering problem from an object with arbitrary shape and surface S. 24
Figure 3.2 Spherical surfaces defined for the interior (S_2) and exterior (S_1) boundaries for the scatterer defined with boundary S. V_1 defines exterior to S and V_2 defines interior to S. 28
Figure 4.1 Field scattered from each element shown of N is translated to group's center and then interactions with elements of M are calculated from the center of N once. Hence, interaction count between groups of elements could be reduced with the

use of multipole elements. (Only several interactions are demonstrated due to clarity) 38
Figure 4.2 Calculation of particle interaction amongst particle located in N and particles distributed in space and demonstrated with M. (Only several interactions are demonstrated due to clarity) 39
Figure 4.3 Computational space is divided into groups. Scattered fields in each group are translated to group center. From the far groups, aggregated fields are translated to target groups one by one (long vectors). At disaggregation step, summation of translated fields is translated to particle location of target group. 40
Figure 4.4 According to required accuracy ε and given δ due to distribution of the scatterers required shift p_0 can be found using error maps obtained using scattering calculation of two spheres. Filled markers demonstrates δ=1.5 condition and hollow markers are for δ=2 condition. Objects under consideration are sound hard spheres with equal dimensions. (Figure is obtained from [35]) 47
Figure 4.5 Relative error of FMM with respect to truncation number $N\alpha$ and group size D. [43] proposes the use of FMM for group size larger than 0.2λ due to increased relative error of the translation step. For smaller group sizes low frequency FMM is recommended. (Figure is obtained from [43]) 49
Figure 4.6 Dielectric sphere is represented as cluster of smaller spheres. Each sphere in cluster has same radius. Total volume of the large scattering body is represented with a number of smaller spheres. 51
Figure 4.7 For various dielectric scatterer radiuses, normalized monostatic RCS is calculated and compared with Mie series solution. (Dots represent the FMM solver results) 52
Figure 4.8 In order to represent dielectric sphere with increasing radius, number of particles should also enhanced. Mesh size is kept constant with increasing dielectric scatterer size. Hence due to $O(r^3)$ increase in volume, mesh count should increase with $O(r^3)$. 53
Figure 4.9 For various dielectric scatterer radius normalized monostatic RCS is calculated and compared with Mie series solution. 54

Figure 4.10 As the dielectric scatterer radius increases, number of unknowns also increases. Hence, with increased number of unknowns iteration count for required converge increases. 55
Figure 4.11 With increasing scatterer's radius, simulation time can be modeled as a second order polynomial. Simulation period is O(*N*) due to near field interactions. Iteration count also increases with *N*. 56
Figure 4.12 With increased number of unknowns, required memory size increases linearly. For direct solvers memory increases with O(N^2). Due to BiCGStab algorithm utilized, increase in memory is O(*N*). 57
Figure 4.13 Simulation results of dielectric sphere with ε_r of 2.25 and radius of 0.75λ. Residual error gradually decreases below 1e-10 at 80th iteration. Normalized monostatic RCS of cluster of spheres are calculated as 1.7238. For residual errors below 1e-3, error in normalized monostatic RCS calculation is below 1%. Hence, 1e-3 can be used as an error threshold value. 58
Figure 4.14 Residual error with respect to iteration count for various dielectric scatterers. With increasing diameter of scatterers, number of unknowns also increases. Hence, for higher number of unknowns, iteration count increases as well. 59
Figure 4.15 Mesh of NASA almond as a cluster of spheres at 1.19GHz is demonstrated. Center of the spheres are 0.04λ apart. Total number of spheres is 453. Monostatic RCS of the almond is simulated in VV and HH planes. 62
Figure 4.16 Comparison of the FMM simulations with the FEKO monostatic RCS for NASA almond at 1.19GHz. Minimum separation between the centers of the spheres is selected as 0.04λ . Radiuses of the spheres are 0.0232λ. Simulation result of horizontal polarization is provided. 63
Figure 4.17 Comparison of the FMM simulations with the FEKO monostatic RCS for NASA almond at 1.19GHz. Minimum separation between the centers of the spheres is selected as 0.04λ . Radiuses of the spheres are 0.0232λ. Simulation result of vertical polarization is provided. 64
Figure 4.18 Comparison of the FMM simulations with the FEKO monostatic RCS for NASA almond at 1.19GHz. Minimum separation between the centers of the

spheres is selected as 0.04λ . Radiuses of the spheres are 0.02λ. Simulation result of vertical polarization is provided. 64
Figure 4.19 Comparison of the FMM simulations with the FEKO monostatic RCS for NASA almond at 1.19GHz. Minimum separation between the centers of the spheres is selected as 0.04λ . Radiuses of the spheres are 0.02λ. Simulation result of vertical polarization is provided. 65
Figure 4.20 Convergence of the FMM results at various angles for monostatic RCS calculation of NASA almond at 1.19GHz. Minimum separation between the centers of the spheres is selected as 0.04λ . Radiuses of the spheres are 0.021λ. Simulation result of horizontal polarization is provided. (For clarity, only results of the selected angles are provided.) 66
Figure 4.21 Demonstration of meshing of a volume using spheres. Selection of sphere radius as half of the mesh size or smaller corresponds to realistic problem. With selection of larger sphere size effects converge of the solver since model represents a fictitious problem. 67
Figure 4.22 Mesh of NASA almond as a cluster of spheres at 7GHz is demonstrated. Center of the spheres are 0.1λ apart. Total number of spheres is 1995. Monostatic RCS of the almond is simulated in VV and HH planes. 68
Figure 4.23 Comparison of the FMM simulations with the measurements of monostatic RCS for NASA almond at 7.0GHz. Minimum separation between the centers of the spheres is selected as 0.1λ . Radiuses of the spheres are 0.058λ. Simulation result of horizontal polarization is provided. Dashed line represents measurement result and solid line denotes FMM result..... 68
Figure 4.24 Comparison of the FMM simulations with the measurements of monostatic RCS for NASA almond at 7.0GHz. Minimum separation between the centers of the spheres is selected as 0.1λ . Radiuses of the spheres are 0.058λ. Simulation result of vertical polarization is provided. Dashed line represents measurement result and solid line denotes FMM result..... 69
Figure 4.25 Comparison of the FMM simulations with the measurements of monostatic RCS for NASA almond at 9.92GHz. Minimum separation between the centers of the spheres is selected as 0.1λ . Radiuses of the spheres are 0.058λ.

Simulation result of horizontal polarization is provided. Dashed line represents measurement result and solid line denotes FMM results [45]. 70
Figure 4.26 Comparison of the FMM simulations with the FEKO simulations of monostatic RCS for NASA almond at 9.92GHz. Minimum separation between the centers of the spheres is selected as 0.1λ . Radiuses of the spheres are 0.058λ. Simulation result of vertical polarization is provided. Line with diamond marker is FMM results. 71

LIST OF ABBREVIATIONS

BICGSTAB	:	Biconjugate Gradient Stabilized
CGS	:	Conjugate Gradient Squared
FDTD	:	Finite Difference Time Domain Method
FEM	:	Finite Element Method
FMM	:	Fast Multipole Method
RCS	:	Radar Cross Section
SOR	:	Succesive Over Relaxation
VIE	:	Volume Integral Equation Method
VSWF	:	Vector Spherical Wave Functions

CHAPTER 1

INTRODUCTION

1.1 Background and Scope

Purpose of this dissertation is to form a fast electromagnetic solver in order to analyze multiple interactions between clusters of scatterers. Hence, solver should cope with near and far field interactions among scatterers. Even though particles smaller than a wavelength are considered, solver should be able to address scatterers with variable sizes. Moreover, materials used for scattering bodies could be changed. Hence, scatterers with variable radius, permittivity, permeability and non-penetrable bodies should be handled with the algorithm. It is assumed that the scatterer centers are well defined with linear, homogeneous and isotropic electrical properties. Same assumptions also hold for background material.

Since solution of a general scattering problem cannot be handled analytically for most of the cases, numerical methods are used to solve electrostatic, electromagnetic and acoustic scattering problems. Several methods proposed in literature for the formulation and analysis of scattering problems, and these can be categorized according to their discretization methods [1]. Finite element method (FEM) [2], finite difference time domain method (FDTD) [3], and volume integral equation method (VIE) [4]-[6] are among the volume discretization methods. Also, surface discretization methods such as MOM take place in literature. Volume equivalence theorems favour broadband operation, suitability to complex geometry and capability of handling inhomogeneous media. Burden of the volume equivalence theorems include increased matrix size compared to surface equivalence theorems. FEM and FDTD methods yield sparse interaction matrices. Hence, solver should be capable of handling sparse matrices. For the surface discretization methods,

interaction matrix is dense. Hence, computational cost is higher due to increased matrix vector multiplications [1].

Acoustic scattering by two spheres is studied by New and Eisler [7]. Electromagnetic scattering from two spheres is investigated by Liang and Lo [8]. However, particles are constrained on z axis. With the work of Brunning and Lo [9] [10] scattering is examined for particles with arbitrary locations and directions. Scattering from spheres is extended to cluster of spheres with a variety of methods. Electromagnetic scattering from cluster of scatterers is handled by Hamid [11]-[13], Mackowski [14] and Daran [15] using iterative computations. Matrix solution approach is used by Borghese[16]-[19]. However, numbers of scattering bodies are restricted to four spheres. Quinted and Krebig [20] also used the same approach and modeled scattering from small scatterer groups. Electromagnetic or acoustic scattering from random scatterer geometries are handled with T-matrix method introduced by Waterman [21]-[24]. However, with increasing number of elements, this method suffers from matrix inversion.

Due to electrically large problems, highly inhomogeneous media or increased frequencies under consideration, number of unknowns could be quite high. Hence, in order to solve such problems with classical methods, even sources of a super computer can be exhausted. Hence, "*faster*" algorithms are required. "Fast" for an electromagnetic solver implies, particle interactions are computed with less than O (N^2) operations. With the use of fast solvers, interactions can be completed with O (N) operations.

When an electromagnetic wave impinges upon a single spherical scatterer, due to the spherical symmetry of the scatterer body, it may be wise to express the incoming and outgoing waves in spherical coordinates. Solutions of the Helmholtz equation can be represented by vector spherical wave functions in spherical coordinates, since they form a basis for the expansion of the radiating fields. Hence, any incoming and outgoing field can be represented in terms of vector spherical wave functions. Since, we have incoming and outgoing waves, which are expressed

in spherical coordinates; it will be easier to apply boundary conditions on the spherical scatterer. However, scattering problems generally include more than single scatterer body. Therefore, we have to apply the boundary conditions not only on a single sphere but also on a cluster of scatterers. The purpose of the use of spherical functions is to apply boundary conditions without much effort. Nevertheless, when more than single scatterer is present, boundary conditions cannot be expressed in spherical coordinates for all scatterers. Here, use of an intermediate step is required to translate expansion centers of the fields. If one can express the incoming and outgoing fields at different coordinate frames then boundary conditions can be used without much effort.

It is possible to express incident fields in terms of vector spherical wave functions. Then, we should be able to express vector wave functions at different coordinate frames. Required tool for this task is vector addition theorem, where vector spherical wave functions at one coordinate frame can be expressed as summation of infinitely many vector spherical wave functions in any other coordinate frame. Hence, basis sets in a coordinate frame can be expressed as infinite summation of a basis set at different location by the use of addition theorems. Basis set for electromagnetic case are the vector spherical wave functions.

T-Matrix formulation (or extended boundary condition method) was introduced by Waterman [21]-[24], and used for the solution of the electrostatic, electromagnetic, acoustic and elastodynamic scattering problems. For an arbitrary shaped scatterer, T-matrix method correlates incoming fields to outgoing fields by use of boundary conditions. Method uses expansion of the internal and external solutions of boundary integral equations on the scattering surface. For electromagnetic scattering, spherical vector wave functions are used to express the fields. Then, integral equations can be represented as summations of vector spherical wave functions (VSWF); hence field interactions can be expressed as matrices. T-matrix relates the coefficients of the outgoing fields to the coefficients of incoming fields. However, expansion includes infinitely many terms and for computational

purposes one should truncate the expansion at a predefined value. Therefore, instead of actual values, approximations of the fields are used.

Throughout this dissertation, scatterers will be treated as small spheres. Size of the spheres will depend on the size of the discretization steps. Calculation of the T-matrix for a spherical scatterer is a trivial step and can be implemented with analytical means. Then, aim is to find the coefficients of the incoming and outgoing vector spherical wave functions.

FMM (Fast Multipole Method) method was introduced by Greengard and Rokhlin [25] and acclaimed as one of the top ten algorithms of 20^{th} century [26]. FMM is developed for the fast summation of the multipole solution of Laplace equation and reduces the computation cost of matrix-vector products of a solver. Scatterers are grouped and interactions between the electrically far groups are treated as if there is a single scatterer in center of each group. Hence, instead of computing the pair wise interactions between the scatterers, interactions between the groups are analyzed. Direct calculation of the interactions for N body problem gives rise to $O(N^2)$ operations, whereas calculation of group interactions will be completed with considerably fewer operations. With multilevel fast multipole method (MLFMM) algorithm computational complexity can be reduced down to $O(N\log N)$ [27], since particle interactions are not formed explicitly.

Direct methods provide exact solution in N number of steps and $O(N^2)$ matrix operations at each step, as in the case of Gaussian elimination. In order to apply direct methods to matrices, they must be stored. Since matrices must be stored, direct methods suffer from increased memory requirement for large systems. On the other hand, iterative algorithms like Bi-Conjugate Gradient Method (BiCG) or Generalized Minimum Residual Method (GMRES), require lower memory. Instead of generating exact solution in N steps, they provide approximate solution in N_{iter} steps. For smaller problems, where matrix inversion is possible, direct methods outperforms since iterative method should be repeated N_{iter} steps to converge with desired accuracy. However, for larger problems, if properly conditioned, N_{iter} can be much less than N.

Also, direct solvers consume excessive amount of memory and for very large problems iterative methods are the only possible option. Iterative solutions generate an approximate solution to a matrix equation. However, with sufficient iteration steps error of the solution can be reduced down to machine precision as in the case of FMM solution.

1.2 Advantages of the Fast Multipole Method

FMM is primarily developed for the accelerated solution of the Laplace equation and based on expansion of the fundamental solution over a basis function. This new method attempts to solve the original problem in an approximate fashion instead of the analytical solution. However, with the proper truncation of the approximation, error levels down to machine precision could be achieved.

Despite the fact that it is developed for the solution of Laplace equation, it can be used in a diversity of scientific computation applications such as solution of electrostatic, magnetostatic, electrodynamics, and particle dynamic problems.

In classical methods, computation cost of pairwise interactions between N scatters is $O(N^2)$, whereas cost reduces to $O(N\log N)$ or $O(N)$ with MLFMM algorithms. Hence, for large clusters of particles, there is a significant reduction in the computation cost of the scattering problems. With the use of iterative algorithms, FMM offers reduced computation duration and memory requirement, compared to classical algorithms like MOM and FEM. Hence substantially larger numerical problems can be solved. Problems which exhaust computer resources with other algorithms can be handled easily with the use of FMM algorithm.

1.3 Diagonalization of Translation Operators in FMM

Translation of the multipoles from the source location to the observation point is accomplished with the use of three addition theorems in FMM rather than a single translation. These are called as aggregation, translation, and disaggregation steps. Prerequisite for such a translation to be possible is that the source and observation points are well separated. Each translation step can be visualized as a matrix-vector multiplication, with a dense matrix. Without proper diagonalization of

the matrix prefactor of O(*N*) complexity can be high and efficiency of the FMM solver can be degraded. Increased complexity results from the translation of the outgoing fields generated by the sources to the observation points as incoming fields. Hence, proper modifications to the translation matrices are required.

With the use of diagonalization, matrix vector multiplication required for the translation step can be diagonalized. However, computation cost related with aggregation and disaggregation steps are not altered with this modification.

1.4 Organization of the Thesis

In chapter 2, vector spherical wave functions are reviewed. With the use of scalar addition theorem, a derivation of vector addition theorem is presented. For the acceleration of the calculation of the vector addition theorem, recurrence relations are also presented. A plane wave is expressed in terms of vector spherical wave functions.

In chapter 3, extended boundary condition method is briefly introduced. T-matrix method and iterative methods are given in this chapter.

In chapter 4, diagonalization of the vector addition theorem is derived. Error sources during the diagonalization process are presented. Finally, numerical results obtained from the implemented code are given. Throughout this thesis $e^{j\omega t}$ time convention is used.

CHAPTER 2

VECTOR SPHERICAL WAVE FUNCTIONS, SCALAR AND VECTOR ADDITION THEOREM

2.1 Introduction

This section intends to give the reader basic knowledge of the functions and theorems given in FMM steps. Addition theorem is one of the core tools for the FMM algorithm.

Translation of the spherical waves from one coordinate system to another is accomplished using addition theorem. Addition theorem is a tool for expressing the basis set in one coordinate system in terms of basis set of another coordinate system. Basis set here is the vector spherical wave functions.

2.2 Vector Spherical Wave Functions

A scalar wave function φ is defined as the solution of Helmholtz equation in spherical coordinates where $\mathbf{r}$ is the position vector and k is the wave number.

$$\nabla^2\varphi + k^2\varphi = 0 \tag{2-1}$$

Using the definitions given in [28], for spherical coordinates scalar wave function φ is given as,

$$\varphi_{nm}(\mathbf{r}) = z_n^q(kr)Y_{nm}(\theta,\phi) \tag{2-2}$$

where r is the radial distance from origin, θ and ϕ are the spherical polar angles.

According to the value of q, z_n^q is selected as one of Bessel or Hankel functions. 1 is for Bessel function of first kind, 2 is for Bessel function of second kind, 3 is for the Hankel function of first kind and 4 is for the Hankel function of second kind.

The electric and magnetic fields in a source-free homogeneous medium are divergence-free and satisfies the vector wave function of the form,

$$\nabla \times \nabla \times \mathbf{A} - k^2 \mathbf{A} = 0 \tag{2-3}$$

where k is the propagation constant. Relation between two independent solutions can be expressed as

$$\begin{aligned} k\mathbf{N} &= \nabla \times \mathbf{M} \\ k\mathbf{M} &= \nabla \times \mathbf{N} \end{aligned} \tag{2-4}$$

Then we construct the following vectors $\mathbf{M}_{nm}$ and $\mathbf{N}_{nm}$,

$$\mathbf{M}_{nm}(\mathbf{r}) = \nabla \times \mathbf{r}\varphi_{nm}(\mathbf{r}) \tag{2-5}$$

$$k\mathbf{N}_{nm}(\mathbf{r}) = \nabla \times \mathbf{M}_{nm}(\mathbf{r}) \tag{2-6}$$

If **M** or **N** is substituted in vector Helmholtz equation, equality holds.

Y_{nm} is the spherical harmonic function. Definition of Y_{nm} is given in (2-7), and modification for negative m given in (2-8) as:

$$Y_{nm}(\theta, \phi) = \sqrt{\frac{2n+1}{4\pi}} \sqrt{\frac{(n-m)!}{(n+m)!}} P_n^m(\cos\,\theta) e^{jm\phi} \tag{2-7}$$

$$Y_{n,-m}(\theta, \phi) = (-1)^m Y_{n,m}^*(\theta, \phi) \tag{2-8}$$

and P_n^m is the associated Legendre function. Explicit expressions are provided in [29] for **M** and **N**. Both of them can be stored as 3x1 complex matrices.

$$\mathbf{M}_{nm}(\mathbf{r}) = \frac{jm}{\sin(\theta)} z_n^q(kr) Y_{nm}(\theta,\phi)\hat{\theta} - z_n^q(kr)\frac{\partial Y_{nm}(\theta,\phi)}{\partial\theta}\hat{\phi} \tag{2-9}$$

$$\mathbf{N}_{nm}(\mathbf{r}) = \frac{n(n+1)}{kr} z_n^q(kr) Y_{nm}(\theta,\phi)\hat{r} - \frac{1}{kr}\left[r z_n^q(kr)\right]\frac{\partial Y_{nm}(\theta,\phi)}{\partial\theta}\hat{\theta} + \frac{jm}{kr\sin(\theta)}\frac{\partial}{\partial r}\left[r z_n^q(kr)\right] Y_{nm}(\theta,\phi)\hat{\phi} \tag{2-10}$$

$\hat{r}, \hat{\theta}, \text{and } \hat{\phi}$ given in above equations denotes the unit vectors in spherical coordinates.

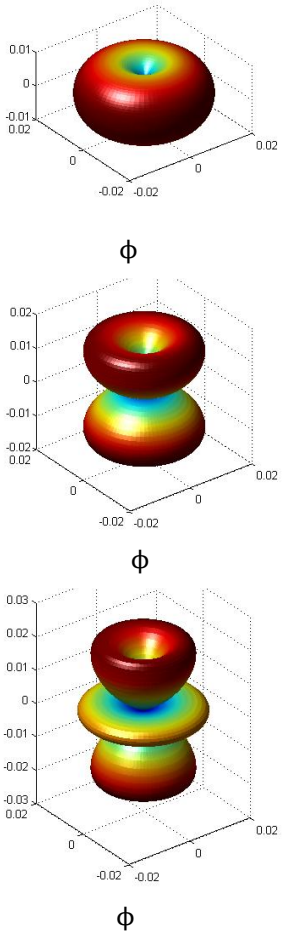

Figure 2.1 Vector representation of **M** fields. (From top to bottom $\mathbf{M}_{10}$, $\mathbf{M}_{20}$, $\mathbf{M}_{30}$ are shown)

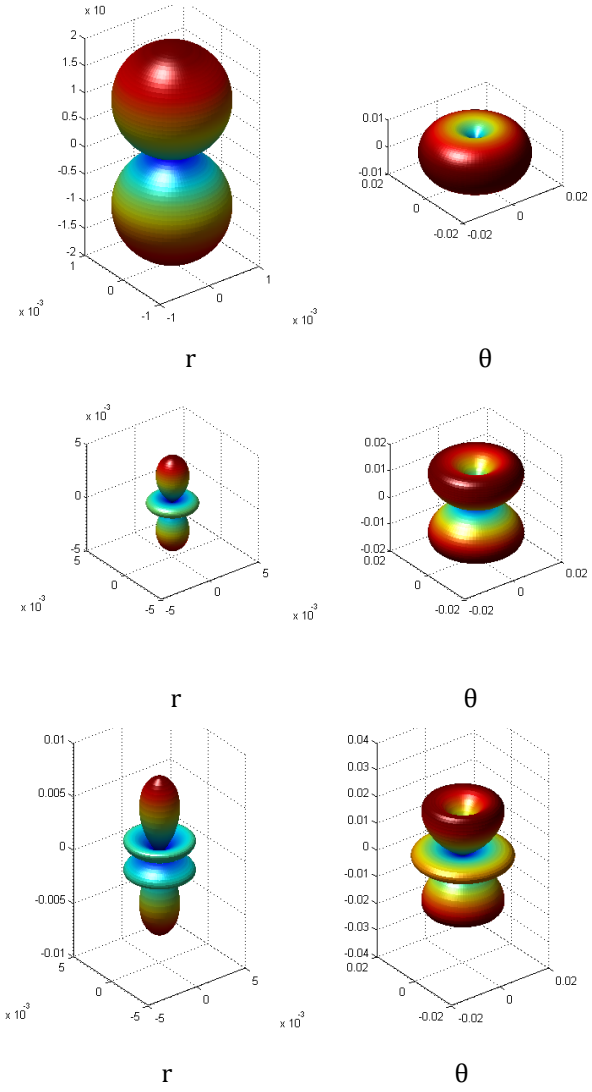

Figure 2.2 Vector representation of **N** fields. From top to bottom $\mathbf{N}_{10}$, $\mathbf{N}_{20}$, $\mathbf{N}_{30}$ are shown)

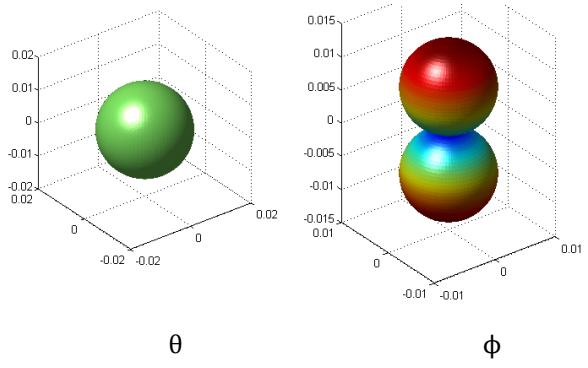

Figure 2.3 Vector representation of $\mathbf{M}_{11}$ field.

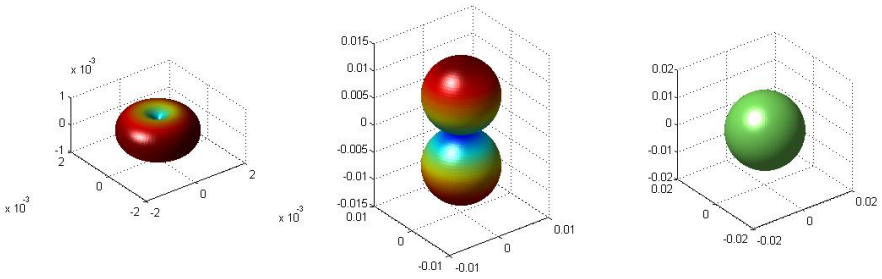

Figure 2.4 Vector representation of $\mathbf{N}_{11}$ field.

Instead of differentiations given in (2-9) and (2-10), analytical formulations are provided in [28], for the radial derivative, as given in (2-11), where prime defines differentiation with respect to kr and can be computed using recurrence relations for Bessel functions (2-12). $f_n(z)$ denotes any of Bessel or Hankel functions.

$$\frac{\partial}{\partial r}\left[r z_n^q(kr)\right] = z_n^q(kr) + kr z_n^{q\prime}(kr) \tag{2-11}$$

$$\frac{n}{z} f_n(z) - \frac{d}{dz} f_n(z) = f_{n+1}(z) \tag{2-12}$$

Using (2-11) and (2-12) following formula is obtained.

$$\frac{1}{kr}\frac{d}{dr}[r f_n(kr)] = \frac{n+1}{kr} f_n(kr) - f_{n+1}(kr) \tag{2-13}$$

Also, recurrence relations for the derivatives of spherical harmonics are given as,

$$\begin{aligned}\frac{\partial Y_{nm}(\theta,\phi)}{\partial\theta} = -\frac{1}{2}\Big[&\sqrt{(n-m+1)(n+m)}\,Y_{n,m-1}e^{j\phi} \\ &- \sqrt{(n+m+1)(n-m)}\,Y_{n,m+1}e^{-j\phi}\Big]\end{aligned} \tag{2-14}$$

where for negative m formulation is modified as,

$$\frac{\partial Y_{n,-m}(\theta,\phi)}{\partial\theta} = (-1)^m \left(\frac{\partial Y_{nm}(\theta,\phi)}{\partial\theta}\right)^* \tag{2-15}$$

Another issue related to computation is the $\sin\theta$ dependency in denominators of (2-9) and (2-10). For $\theta \to n\pi$ where n is an integer, computation can end up with ambiguous results. For $\theta = n\pi \mp \pi/8$ following equation can be used.

$$\frac{Y_{nm}(\theta,\phi)}{\sin\theta} = -\frac{1}{2m\cos\theta}\left[\sqrt{(n-m)(n+m+1)}\,Y_{n,m+1}e^{-j\phi} + \sqrt{(n+m)(n-m+1)}\,Y_{n,m-1}e^{j\phi}\right] \tag{2-16}$$

Recursion formulas for the derivative of the Associated legendre function can be written as,

$$\frac{\partial P_n^m}{\partial\theta} = -\frac{1}{2}[(n-m+1)(n+m)P_n^{m-1} - P_n^{m+1}] \tag{2-17}$$

2.3 Scalar and Vector Translational Addition Theorems

Consider a scatterer located at a point in space with coordinates (r,θ,ϕ). In order to apply boundary conditions easily to a spherical scatterer located at this point we should translate the fields to this new coordinate axes. Define the new coordinate axes such that center is located at (r,θ,ϕ). Also, orient the new axes such that $\theta' = 0 \text{ and}, \phi' = 0$ is parallel to the previous axes $\theta = 0 \text{ and}, \phi = 0$. This type of translation is called a rigid translation.

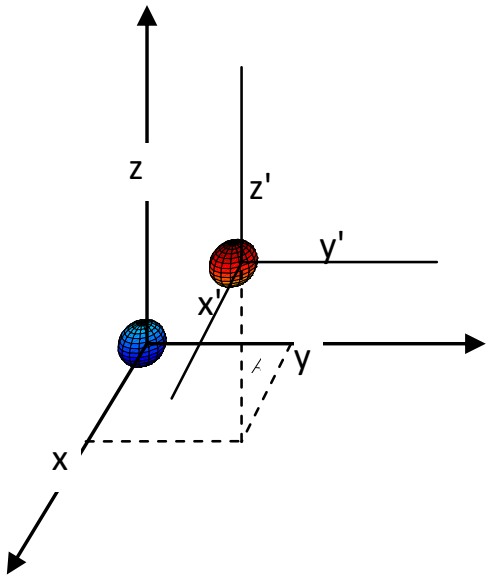

Figure 2.5 Translation of the coordinate axes to new coordinate frame located at (r, θ, ϕ).

According to [29], solution of the scalar Helmholtz equation can be expressed in a different coordinate frame as:

$$z_n^q(kr)Y_{nm}(\theta,\phi) = \sum_{n'=0}^{\infty} \sum_{m'=-n}^{n} \alpha_{n,m,n'm'}\, z_{n'}^{q_1}(kr')Y_{n',m'}(\theta',\phi') \qquad (2\text{-}18)$$

where $\mathbf{r} = \mathbf{r'} + \mathbf{r''}$. q_1 is selected according to the magnitudes of r' and r''. For $r'>r''$ $q_1 = q$. Otherwise, q_1=1. $\mathbf{r''}$ is the vector from the center of the unprimed coordinate system to the center of the primed coordinate system, i.e., it is the vector that defines the translation.

Scalar addition theorem is not used in electromagnetic problems and we are primarily concerned with vector translational addition theorem [28]. Scalar addition theorem will be used for recursion formulas of the vector addition theorem.

The translational addition theorem for the vector case can be written as:

$$\mathbf{M}_{nm}^{q}(\mathbf{r}) = \sum_{n'=1}^{\infty} \sum_{m'=-n}^{n} A_{n'm',nm}\, \mathbf{M}_{n'm'}^{q_1}(\mathbf{r}') + B_{n'm',nm} \mathbf{N}_{n'm'}^{q_1}(\mathbf{r}') \tag{2-19}$$

$$\mathbf{N}_{nm}^{q}(\mathbf{r}) = \sum_{n'=1}^{\infty} \sum_{m'=-n}^{n} A_{n'm',nm}\, \mathbf{N}_{n'm'}^{q_1}(\mathbf{r}') + B_{n'm',nm} \mathbf{M}_{n'm'}^{q_1}(\mathbf{r}') \tag{2-20}$$

q_1 is selected according to the magnitudes of r′ and r″. For r′> r″, $q_1 = q$. Otherwise, $q_1 = 1$.

Constants given in above equations are defined as:

$$A_{n'm',nm} = \frac{\alpha_{nm,n'm'}^{A}}{2n'(n+1)} \tag{2-21}$$

$$\alpha_{nm,n'm'}^{A} = 4\pi(i)^{n'-n}(-1)^{m} \sum_{l''} \alpha'_{A}(n, n', m, -m', l'')\, z_{l''}^{q_2}(kr'') Y_{l'',m-m'}(\theta'', \phi'') \tag{2-22}$$

This case q_2 has the reverse order of q_1. For r′> r″ q_2=1. Otherwise, $q_2 = q$.

$$\begin{aligned} &\alpha'_{A}(n, n', m, -m', l'') \\ &\quad = [n(n+1) + n'(n'+1) \\ &\quad - l''(l''+1)]a'(n, n'm, -m', l'') \end{aligned} \tag{2-23}$$

$$\begin{aligned} &a'(n, n'm, m', l'') \\ &\quad = [(2n+1)(2n'+1)(2l''+1) \\ &\quad /4\pi]^{1/2} \begin{pmatrix} n & n' & l'' \\ 0 & 0 & 0 \end{pmatrix} \begin{pmatrix} n & n' & l'' \\ m & m' & -m-m' \end{pmatrix} \end{aligned} \tag{2-24}$$

where $\begin{pmatrix} a_1 & a_2 & a_3 \\ b_1 & b_2 & b_3 \end{pmatrix}$ are the Wigner 3-j coefficients [29].

$$B_{n'm',nm} = \frac{jkr''\cos\theta''}{2n'(n+1)} 2m'\alpha_{nm,n'm'} + \frac{jkr''\sin\theta''}{2n'(n+1)} (e^{i\phi''}[(n'-m')(n'+m'+1)]^{\frac{1}{2}}\alpha_{nm,n'm'+1} + e^{-j\phi''}[(n'+m')(n'-m'+1)]^{\frac{1}{2}}\alpha_{nm,n'm'-1}) \quad (2\text{-}25)$$

$$\alpha_{nm,n'm'} = 4\pi(j)^{n'-n}(-1)^{m}\sum_{l''}(j)^{l''}a'(n,n',m,-m',l'')\, z_{l''}^{q_2}(kr'')Y_{l'',m-m'}(\theta'',\phi'') \quad (2\text{-}26)$$

For $r' > r''$ $q_2 = 1$ and otherwise, $q_2 = q$.

Since there are too many terms to be calculated in each translation, translation procedure consumes high CPU time. Therefore, efficiency of the calculation of the translation coefficients plays significant role both in the scalar case and in the vector translational addition theorems. Hence, translation of the vector waves constitutes the major computation time of the electromagnetic solver. Recurrence relations are used for reducing the calculation speed of the translation coefficients.

2.4 Recurrence Relations for Vector Addition Theorem

Recurrence relations for the computation of translation coefficients reduce the complexity of the calculations and decrease the simulation time several orders of magnitude.

Recurrence relations exist for the scalar case. A detailed procedure for the computation of the scalar coefficients are presented in [48]. Using similar procedure and equations given in [28], we may construct the necessary vector recurrence translation coefficients. Explanation of this procedure is given in [28].

Scalar addition theorem can be expressed as:

$$\varphi_{nm}(\mathbf{r}) = \sum_{v=0}^{\infty} \sum_{\mu=-v}^{v} \beta_{v\mu,nm}\, \varphi_{v\mu}(\mathbf{r}') \tag{2-27}$$

where $\beta_{v\mu,nm}$ are the scalar translation coefficients. Notice that scalar translation coefficients are the regular parts of the vector translation coefficients that are given in (2-18). Initial values of these scalar coefficients are provided in [48] as:

$$\beta_{v\mu,00} = (-1)^{v+\mu}\sqrt{4\pi} Y_{v,-\mu}(\theta'', \phi'') z_n^q(kr'') \tag{2-28}$$

Starting with the given initial scalar coefficients, rest of the coefficients for the scalar addition theorem can be calculated recursively. The recursive relations for the coefficients of the vector addition theorem are also derived in the literature. Since detailed derivations are provided in [28], only the results of the derivations are presented here.

$$A_{v\mu,10} = \sqrt{3}\left(z^{+}_{v-1,\mu}\beta_{v-1,\mu,00} + z^{-}_{v+1,\mu}\beta_{v+1,\mu,00}\right) \tag{2-29}$$

$$B_{v\mu,10} = \sqrt{3} z^{0}_{v,\mu}\beta_{v,\mu,00} \tag{2-30}$$

$$z^{0}_{v\mu} = \frac{j\mu}{v(v+1)} \tag{2-31}$$

$$z^{-}_{v\mu} = \frac{a^{-}_{v\mu}}{v} \tag{2-32}$$

$$z^{+}_{v\mu} = -\frac{a^{+}_{v\mu}}{v+1} \tag{2-33}$$

$$a^{-}_{v\mu} = \left[\frac{(v+\mu)(v-\mu)}{(2v+1)(2v-1)}\right]^{\frac{1}{2}} \tag{2-34}$$

$$a_{v\mu}^{+} = -\left[\frac{(v+\mu+1)(v-\mu+1)}{(2v+1)(2v+3)}\right]^{\frac{1}{2}} \tag{2-35}$$

$$A_{v\mu,11} = -\sqrt{\frac{3}{2}}\left(\eta_{v+1\mu-1(+)}^{-}\beta_{v+1,\mu-1,00} + \eta_{v-1\mu-1(+)}^{+}\beta_{v-1,\mu-1,00}\right) \tag{2-36}$$

$$B_{v\mu,11} = -\sqrt{\frac{3}{2}}\eta_{v,\mu-1(+)}^{0}\beta_{v,\mu-1,00} \tag{2-37}$$

$$\eta_{v,\mu(\pm)}^{0} = \frac{j\sqrt{(v\mp\mu)(v\pm\mu+1)}}{v(v+1)} \tag{2-38}$$

$$\eta_{v,\mu(\pm)}^{+} = -\frac{b_{v\mu(\pm)}^{+}}{v+1} \tag{2-39}$$

$$\eta_{v,\mu(\pm)}^{-} = \frac{b_{v\mu(\pm)}^{-}}{v} \tag{2-40}$$

$$b_{v\mu(\pm)}^{+} = \pm\left[\frac{(v\pm\mu+2)(v\pm\mu+1)}{(2v+1)(2v+3)}\right]^{\frac{1}{2}} \tag{2-41}$$

$$b_{v\mu(\pm)}^{-} = \pm\left[\frac{(v\mp\mu)(v\mp\mu-1)}{(2v+1)(2v-1)}\right]^{\frac{1}{2}} \tag{2-42}$$

Two more sets of initial equations are required in order to compute every element with recursion formulas. Derivations are not given in [28], nevertheless, derivation is simple and only the results will be provided here.

$$A_{v\mu,1-1} = \sqrt{\frac{3}{2}}\left(\eta_{v+1\mu+1(-)}^{-}\beta_{v+1,\mu+1,00} + \eta_{v-1\mu+1(-)}^{+}\beta_{v-1,\mu+1,00}\right) \tag{2-43}$$

$$B_{v\mu,1-1} = \sqrt{\frac{3}{2}}\eta_{v,\mu+1(-)}^{0}\beta_{v,\mu+1,00} \tag{2-44}$$

After completing calculation of the initial values given by (2-29), (2-30), (2-36), (2-37), (2-43),and (2-44), to generate higher order terms we need to have recursion formulas for $A_{v\mu,nm}$ and $B_{v\mu,nm}$.

$$\gamma^{+}_{nn}A_{v\mu,n+1,n+1} = \gamma^{-}_{v+1,\mu-1}A_{v+1\mu-1,n,n} + \gamma^{+}_{v-1,\mu-1}A_{v-1\mu-1,n,n} + \gamma^{0}_{v,\mu-1}B_{v,\mu-1,n,n} \tag{2-45}$$

$$\gamma^{+}_{nn}B_{v\mu,n+1,n+1} = \gamma^{-}_{v+1,\mu-1}B_{v+1\mu-1,n,n} + \gamma^{+}_{v-1,\mu-1}B_{v-1\mu-1,n,n} + \gamma^{0}_{v,\mu-1}A_{v,\mu-1,n,n} \tag{2-46}$$

$$\gamma^{0}_{v,\mu} = \frac{j\sqrt{(v-\mu)(v+\mu+1)}}{v(v+1)} \tag{2-47}$$

$$\gamma^{-}_{v,\mu} = \frac{v+1}{v}b^{-}_{v\mu(+)} \tag{2-48}$$

$$\gamma^{+}_{v,\mu} = \frac{v}{v+1}b^{+}_{v\mu(+)} \tag{2-49}$$

$$\lambda^{+}_{nm}A_{v\mu,n+1,m} + \lambda^{-}_{nm}A_{v\mu,n-1,m} + \lambda^{0}_{nm}B_{v\mu,nm} = \lambda^{+}_{v-1,\mu}A_{v-1,\mu,n,m} + \lambda^{-}_{v+1,\mu}A_{v+1,\mu,n,m} + \lambda^{0}_{v\mu}B_{v\mu,nm} \tag{2-50}$$

$$\lambda^{+}_{nm}B_{v\mu,n+1,m} + \lambda^{-}_{nm}B_{v\mu,n-1,m} + \lambda^{0}_{nm}A_{v\mu,nm} = \lambda^{+}_{v-1,\mu}B_{v-1,\mu,n,m} + \lambda^{-}_{v+1,\mu}B_{v+1,\mu,n,m} + \lambda^{0}_{v\mu}A_{v\mu,nm} \tag{2-51}$$

$$\lambda^{0}_{v\mu} = \frac{j\mu}{v(v+1)} \tag{2-52}$$

$$\lambda^{-}_{v\mu} = \frac{v+1}{v}a^{-}_{v\mu} \tag{2-53}$$

$$\lambda^{+}_{v\mu} = \frac{v}{v+1} a^{+}_{v\mu} \tag{2-54}$$

Similar formulas for negative subscripts can also be generated. Although their derivations are not given in [28], it is straightforward and only the results are provided here:

$$\gamma^{+}_{nm-} A_{v\mu,n+1,-(n+1)} = \gamma^{-}_{v+1,\mu+1(-)} A_{v+1\mu+1,n,-n} + \gamma^{+}_{v-1,\mu+1(-)} A_{v-1\mu+1,n,-n} + \gamma^{0}_{v,\mu+1(-)} B_{v,\mu+1,n,-n} \tag{2-55}$$

$$\gamma^{+}_{nm-} B_{v\mu,n+1,-(n+1)} = \gamma^{-}_{v+1,\mu+1(-)} B_{v+1\mu+1,n,-n} + \gamma^{+}_{v-1,\mu+1(-)} B_{v-1\mu+1,n,-n} + \gamma^{0}_{v,\mu+1(-)} A_{v,\mu+1,n,-n} \tag{2-56}$$

where we define new constants as:

$$\gamma^{-}_{n,m-} = \frac{n+1}{n} b^{-}_{nm-} \tag{2-57}$$

$$\gamma^{+}_{n,m-} = \frac{n}{n+1} b^{+}_{nm-} \tag{2-58}$$

$$\gamma^{0}_{n,m-} = \frac{j\sqrt{(n+m)(n-m+1)}}{n(n+1)} \tag{2-59}$$

Recursion formulas (2-45) and (2-46) are used for recursive calculations where n and m increase together. Hence using initial values and recursion formulas $A_{v\mu,2,2}$, $A_{v\mu,3,3}$, $A_{v\mu,4,4}$, … can be calculated. Same is also true for $B_{v\mu,nm}$. In Figure 2.6 effect of the recursion formula is demonstrated as a vector along the diagonal.

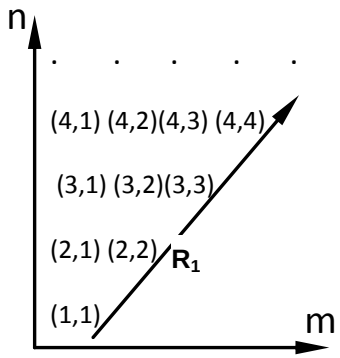

Figure 2.6 Translation coefficient calculation for increasing n and m. Translation coefficients along the diagonal shown in figure with vector R_1 is calculated using the initial values $\beta_{\nu\mu,00}$ and recursion formulas (2-45) and (2-46).

Recursion formulas (2-55) and (2-56) are used for recursive calculations where n and -m increase together. Hence using initial values and recursion formulas $A_{\nu\mu,2,-2}$, $A_{\nu\mu,3,-3}$, $A_{\nu\mu,4,-4}$, … can be calculated. Same is also true for $B_{\nu\mu,nm}$. In Figure 2.7 effect of the recursion formulas (2-55) and (2-56) is demonstrated as a vector along the diagonal.

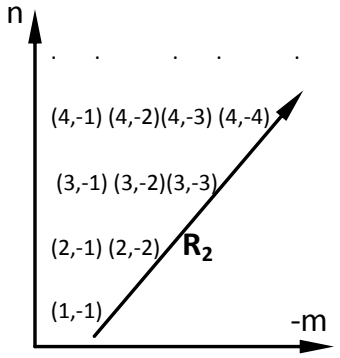

Figure 2.7 Translation coefficient calculation for increasing n and m. Translation coefficients along the diagonal shown in figure with vector R_2 is calculated using the initial values $\beta_{\nu\mu,00}$ and recursion formulas (2-55) and (2-56).

With the use of the given recursion formulas (2-45), (2-46), (2-55) and (2-56) it is only possible to move along the diagonals as shown in Figure 2.6 and Figure 2.7. Hence, another set of recursion formula is used for moving along the columns of the translation coefficients which are given in (2-50) and (2-51). With the use of final set

of equations, starting from the diagonal element of the same column, required translation coefficients can be recursively computed.

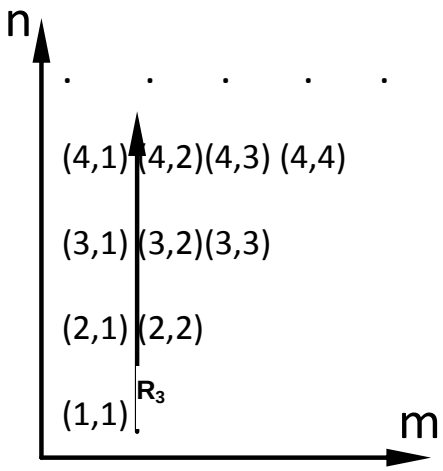

Figure 2.8 Translation coefficient calculations for increasing n and constant m. Column vector shown in figure with vector R_3 is calculated by the recursion formulas (2-50) and (2-51) with the use of the initial values along the diagonal vectors R_1 and R_2.

As an example, to compute the translation coefficient $A_{v\mu,6,-3}$ following steps should be applied.

i) Use recursion formulas (2-55) and (2-56) to obtain $A_{v\mu,2,-2}$ and $A_{v\mu,3,-3}$.

ii) Use recursion formulas (2-50) and (2-51) to obtain $A_{v\mu,4,-3}$, $A_{v\mu,5,-3}$ and $A_{v\mu,6,-3}$.

In order to compute translation coefficient $B_{v\mu,6,4}$ following steps should be applied.

iii) Use recursion formulas (2-45) and (2-46) to obtain $B_{v\mu,2,2}$, $B_{v\mu,3,3}$ and $B_{v\mu,4,4}$.

iv) Use recursion formulas (2-50) and (2-51) to obtain $B_{v\mu,5,4}$ and $B_{v\mu,6,4}$.

2.4.1 Multipole Expansion of a Plane Wave

Consider an x polarized plane wave propagating in the z direction, where $\hat{x}$ is the unit vector along x axis.

$$\mathbf{E}(\mathbf{r}) = \mathrm{E}_0 \hat{\mathrm{x}} \mathrm{e}^{-\mathrm{jkz}} \tag{2-60}$$

We can expand the field in terms of $\mathbf{M}_{\mathrm{n,m}}$ and $\mathbf{N}_{\mathrm{n,m}}$ functions since $\mathbf{E}(\mathbf{r})$ is divergence free. Also, since incoming field is regular at the origin, we can use $\mathrm{z}_{\mathrm{n}}^{1}$ which is the spherical Bessel function of first kind. Hence express the incoming waves as:

$$\mathbf{E}(\mathbf{r}) = \sum_{\mathrm{n}=1}^{\infty} \mathrm{A}_{\mathrm{n,m}} \mathbf{M}_{\mathrm{n,m}}^{\mathbf{1}} + \mathrm{B}_{\mathrm{n,m}} \mathbf{N}_{\mathrm{n,m}}^{\mathbf{1}} \tag{2-61}$$

In order to find the unknown $\mathrm{A}_{\mathrm{n,m}}$ and $\mathrm{B}_{\mathrm{n,m}}$ coefficients one should use the orthogonality of the spherical vector wave functions and results are given in equation (2-62).

$$\mathbf{E}(\mathbf{r}) = -\sum_{\mathrm{n}=1}^{\infty} (-\mathrm{i})^{\mathrm{n}+1} \sqrt{\frac{\pi(2\mathrm{n}+1)}{\mathrm{n}(\mathrm{n}+1)}} \left[\mathbf{M}_{\mathrm{n},1}^{1}(\mathbf{r}) + \mathbf{M}_{\mathrm{n},-1}^{1}(\mathbf{r}) - \mathbf{N}_{\mathrm{n},1}^{1}(\mathbf{r}) + \mathbf{N}_{\mathrm{n},-1}^{1}(\mathbf{r})\right] \tag{2-62}$$

For simplicity define a new function:

$$\bar{\mathbf{\Psi}}(\mathbf{r}) = [\mathbf{M}(\mathbf{r}) \quad \mathbf{N}(\mathbf{r})] \tag{2-63}$$

and rewrite the equation (2-62) as:

$$\mathbf{E}(\mathbf{r}) = \bar{\mathbf{\Psi}}^{1}(\mathbf{r}) \cdot \mathbf{a} \tag{2-64}$$

where **a** is the matrix representation of the coefficients for the expansion.

CHAPTER 3

T-MATRIX FORMULATION

3.1 Introduction

This section intends to give the reader detailed information on the electromagnetic scattering from arbitrary scatterers. T-matrix method will be used for the scattering calculation, which is a consequence of the extended boundary condition method.

For an arbitrary scatterer, T-matrix method correlates the incident and scattered waves. Vector integral equations representing internal and external fields are evaluated on spheres close to the surface of the scatterer. Since the spherical vector wave functions are a complete set, fields can be represented by a summation of vector spherical wave functions.

T-Matrix formulation (or extended boundary condition method) is used for the solution of the electrostatic, electromagnetic, acoustic and elastodynamic scattering problems. This method uses an expansion of the internal and external solutions of boundary integral equations on the scattering surface.

T-matrix method is a powerful tool for the solution of problems with electrically large scattering problems. For the solution of electrically large problems, we will approximate the scatterer body by a conglomerate of small dielectric spheres. Size of the spheres depends on the size of the discretization steps. Thus, since scatterer is a sphere, its T-matrix can be easily computed. Then, aim is to find the coefficient of the incoming and outgoing spherical vector wave functions.

3.2 Surface Integral Equations

Surface integral equations are used for the solution of electromagnetic field analysis of arbitrarily shaped scatterers. Scatterers can be metallic or dielectric. With the use of divergence theorem, surface integral equations reduce the dimension of the problem. For 3 dimensional electromagnetic problems, instead of volume integrations, we deal with surface integrals on the boundaries of the object [30].

3.2.1 Surface Integral Equations for the Electromagnetic Problems

Consider the problem geometry given in Figure 3.1. Constitutive parameters of the body are given as ε_2, μ_2, and σ_2. Surrounding material has constitutive parameters of ε_1, μ_1, and σ_1.

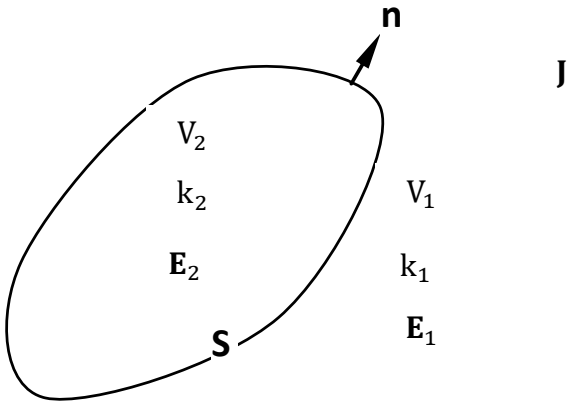

Figure 3.1 Electromagnetic scattering problem from an object with arbitrary shape and surface S.

Vector electromagnetic fields in the region denoted by V_1 satisfy the vector equation given in (3-1).

$$\nabla \times \nabla \times \mathbf{E}_1(\mathbf{r}) - k_1^2 \mathbf{E}_1(\mathbf{r}) = j\omega\mu_1 \mathbf{J}(\mathbf{r}) \tag{3-1}$$

Vector electromagnetic fields in region denoted by V_2 satisfy the vector equation given in (3-2).

$$\nabla \times \nabla \times \mathbf{E}_2(\mathbf{r}) - k_2^2 \mathbf{E}_2(\mathbf{r}) = 0 \tag{3-2}$$

Green's functions defined in each region satisfy the following equations:

$$\nabla \times \nabla \times \bar{\mathbf{G}}_1(\mathbf{r},\mathbf{r}') - k_1^2 \bar{\mathbf{G}}_1(\mathbf{r},\mathbf{r}') = \bar{\mathbf{I}}\delta(\mathbf{r}-\mathbf{r}') \tag{3-3}$$

$$\nabla \times \nabla \times \bar{\mathbf{G}}_2(\mathbf{r},\mathbf{r}') - k_2^2 \bar{\mathbf{G}}_2(\mathbf{r},\mathbf{r}') = \bar{\mathbf{I}}\delta(\mathbf{r}-\mathbf{r}') \tag{3-4}$$

Taking the dot product of (3-3) with $\mathbf{E}_1(\mathrm{r})$ and (3-1) with $\bar{\mathbf{G}}_1(\mathrm{r},\mathrm{r}')$, subtracting the two equations and then integrating over a volume V_1 yields:

$$\begin{aligned} &\oint_{V_1} dv \left(\nabla \times \nabla \times \mathbf{E}_1(\mathbf{r}) \cdot \bar{\mathbf{G}}_1(\mathbf{r},\mathbf{r}') - \mathbf{E}_1(\mathbf{r}) \cdot \nabla \times \nabla \times \bar{\mathbf{G}}_1(\mathbf{r},\mathbf{r}')\right) \\ &\qquad = j\omega\mu_1 \oint_{V_1} dv\ \mathbf{J}(\mathbf{r}) \cdot\ \bar{\mathbf{G}}_1(\mathbf{r},\mathbf{r}') - \mathbf{E}_1(\mathbf{r}') \end{aligned} \tag{3-5}$$

Using the dyadic identities given below in (3-5) ,

$$\begin{aligned} &\nabla \cdot [(\nabla \times \mathbf{E}_1) \times \bar{\mathbf{G}}_1 + \mathbf{E}_1 \times (\nabla \times \bar{\mathbf{G}}_1)] \\ &\qquad = \nabla \times \nabla \times \mathbf{E}_1 \cdot \bar{\mathbf{G}}_1 - \mathbf{E}_1 \cdot \nabla \times \nabla \times \bar{\mathbf{G}}_1 \end{aligned} \tag{3-6}$$

and using divergence theorem results in,

$$\begin{aligned} &-\oint_S ds\, \mathbf{n} \cdot \left(\nabla\left(\nabla \times \mathbf{E}_1(\mathbf{r})\right) \times\ \bar{\mathbf{G}}_1(\mathbf{r},\mathbf{r}') + \mathbf{E}_1(\mathbf{r}) \times \left(\nabla \times\ \bar{\mathbf{G}}_1(\mathbf{r},\mathbf{r}')\right)\right) \\ &\qquad = \mathbf{E}_{\mathrm{inc}}(\mathbf{r}') - \mathbf{E}_1(\mathbf{r}') \end{aligned} \tag{3-7}$$

where $\mathbf{E}_{\mathrm{inc}}$ is the field due to sources $\mathbf{J}(\mathbf{r})$ radiating in the absence of the scattering object with the assumption that $\bar{\mathbf{G}}_1$ is the free space Green's function and $\mathbf{n}$ is the surface normal vector.

$$E_{\mathrm{inc}}(\mathbf{r}') = j\omega\mu_1 \oint_{V1} dV\ \mathbf{J}(\mathbf{r})\, \bar{\mathbf{G}}_1(\mathbf{r},\mathbf{r}') \tag{3-8}$$

Rearranging the terms given in (3-7),

$$\mathbf{E}_1(\mathbf{r}') = \oint_S ds\, \mathbf{n} \cdot \left[\left(\nabla \times \mathbf{E}_1(\mathbf{r})\right) \times \bar{\mathbf{G}}_1(\mathbf{r}, \mathbf{r}') + \mathbf{E}_1(\mathbf{r}) \times \left(\nabla \times \bar{\mathbf{G}}_1(\mathbf{r}, \mathbf{r}')\right)\right] + \mathbf{E}_{\text{inc}}(\mathbf{r}') \tag{3-9}$$

Substituting the following equations in (3-9),

$$\mathbf{n} \cdot \left[\left(\nabla \times \mathbf{E}_1(\mathbf{r})\right) \times \bar{\mathbf{G}}_1(\mathbf{r}, \mathbf{r}')\right] = \bar{\mathbf{G}}_1(\mathbf{r}, \mathbf{r}') \cdot \mathbf{n} \times (-j\omega\mu_1 \mathbf{H}_1(\mathbf{r})) \tag{3-10}$$

$$\mathbf{n} \cdot \left[\mathbf{E}_1(\mathbf{r}) \times \left(\nabla \times \bar{\mathbf{G}}_1(\mathbf{r}, \mathbf{r}')\right)\right] = \left(\nabla \times \bar{\mathbf{G}}_1(\mathbf{r}, \mathbf{r}')\right) \cdot \mathbf{n} \times \mathbf{E}_1(\mathbf{r})) \tag{3-11}$$

$$\bar{\mathbf{G}}_1^{\text{t}}(\mathbf{r}, \mathbf{r}') = \bar{\mathbf{G}}_1(\mathbf{r}', \mathbf{r}) \tag{3-12}$$

$$[\nabla \times \bar{\mathbf{G}}_1(\mathbf{r}, \mathbf{r}')]^{\text{t}} = -\nabla \times \bar{\mathbf{G}}_1(\mathbf{r}', \mathbf{r}) \tag{3-13}$$

we can rewrite equation (3-9) as,

$$\mathbf{E}_1(\mathbf{r}') = \mathbf{E}_{\text{inc}}(\mathbf{r}') + \oint_S ds\left([j\omega\mu_1 \bar{\mathbf{G}}_1(\mathbf{r}', \mathbf{r}) \cdot \mathbf{n} \times \mathbf{H}_1(\mathbf{r})] - \left[\left(\nabla \times \bar{\mathbf{G}}_1(\mathbf{r}', \mathbf{r})\right) \cdot \mathbf{n} \times \mathbf{E}_1(\mathbf{r})\right]\right), \mathrm{r}' \in \mathrm{V}_1 \tag{3-14}$$

Left hand side of the equation given in (3-14) is equal to zero if it is evaluated outside the volume V_1. Hence, after interchanging $\mathbf{r}'$ and $\mathbf{r}$, complete equation system will be,

$$\left.\begin{matrix}\mathbf{r}\epsilon V_1, \mathbf{E}_1(\mathbf{r}) \\ \mathbf{r}\epsilon V_2, \quad 0\end{matrix}\right\} = \mathbf{E}_{\text{inc}}(\mathbf{r}') + \oint_S ds\big([j\omega\mu_1 \bar{\mathbf{G}}_1(\mathbf{r}', \mathbf{r}) \cdot \mathbf{n} \times \mathbf{H}_1(\mathbf{r})] - \big[\big(\nabla \times \bar{\mathbf{G}}_1(\mathbf{r}', \mathbf{r})\big) \cdot \mathbf{n} \times \mathbf{E}_1(\mathbf{r})\big]\big) \tag{3-15}$$

Similar set of equations can be formed for the case in (3-2) and (3-4) yielding,

$$\left.\begin{matrix}\mathbf{r}\epsilon V_1, \mathbf{E}_2(\mathbf{r}) \\ \mathbf{r}\epsilon V_2, \quad 0\end{matrix}\right\} = -\oint_S ds \begin{pmatrix} [j\omega\mu_2 \bar{\mathbf{G}}_2(\mathbf{r}', \mathbf{r}) \cdot \mathbf{n} \times \mathbf{H}_2(\mathbf{r})] \\ -\big[\big(\nabla \times \bar{\mathbf{G}}_2(\mathbf{r}', \mathbf{r})\big) \cdot \mathbf{n} \times \mathbf{E}_2(\mathbf{r})\big] \end{pmatrix} \tag{3-16}$$

Another set of equations comes from the boundary conditions for a dielectric scatterer on S as,

$$\mathbf{n} \times \mathbf{E}_1(\mathbf{r}) = \mathbf{n} \times \mathbf{E}_2(\mathbf{r}) \tag{3-17}$$

$$\mathbf{n} \times \mathbf{H}_1(\mathbf{r}) = \mathbf{n} \times \mathbf{H}_2(\mathbf{r}) \tag{3-18}$$

Hence using (3-17) and (3-18), in null parts of the equations (3-16) and (3-15), we finally obtain integral field equations as,

$$\mathbf{E}_{\text{inc}}(\mathbf{r}) = \oint_S ds\big([j\omega\mu_1 \bar{\mathbf{G}}_1(\mathbf{r}', \mathbf{r}) \cdot \mathbf{n} \times \mathbf{H}_1(\mathbf{r})] - \big[\big(\nabla \times \bar{\mathbf{G}}_1(\mathbf{r}', \mathbf{r})\big) \cdot \mathbf{n} \times \mathbf{E}_1(\mathbf{r})\big]\big) \tag{3-19}$$

$$0 = \oint_S ds\,([j\omega\mu_2\, \bar{\mathbf{G}}_2(\mathbf{r}, \mathbf{r}') \cdot \mathbf{n} \times \mathbf{H}_1(\mathbf{r}')] - [(\nabla \times \bar{\mathbf{G}}_2(\mathbf{r}, \mathbf{r}')) \cdot \mathbf{n} \times \mathbf{E}_1(\mathbf{r}')] \tag{3-20}$$

Once (3-19) and (3-20) are solved for the unknowns, fields inside the volumes can be computed using equations (3-16) and (3-15). For other types of scatterers, with the use of appropriate boundary conditions, necessary integral equations can be obtained.

3.3 Extended Boundary Condition Method

Surface integral equations involved in previous section don't have closed form expressions, unless they can be expressed in a curvilinear coordinate frame. Hence, the surface involved need to be meshed and problem should be solved numerically. Possible candidates for numerical solution could be MOM or FEM. Another method was proposed by Waterman [21]-[24], which is called extended boundary condition method or null-field approach for the solution of given surface integral equations. In the extended boundary conditions method, boundary conditions are not imposed on the surface of S but on two hypothetical spherical surfaces, S_1 and S_2 shown in Figure 3.2, in order to simplify the integral equations. Hence, method provides not the exact solution but an approximation of it. However, it has been shown that the solution is exact if the Rayleigh hypothesis holds [30].

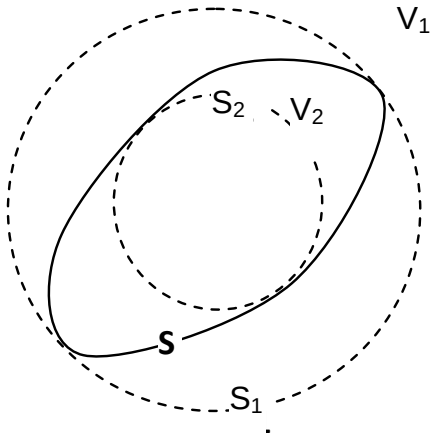

Figure 3.2 Spherical surfaces defined for the interior (S_2) and exterior (S_1) boundaries for the scatterer defined with boundary S. V_1 defines exterior to S and V_2 defines interior to S.

As given in (2-64), the incident field can be expressed as summation of regular spherical vector wave functions.

Unbounded homogeneous-medium Green's function can be written as [31]:

$$\bar{\mathbf{G}}(\mathbf{r},\mathbf{r}') = \mathrm{jk}\sum_{\mathrm{n}} \bar{\boldsymbol{\Psi}}_{\mathrm{n}}^{1}(\mathbf{r})\,\bar{\boldsymbol{\Psi}}_{\mathrm{n}}^{4}(\mathbf{r}') \tag{3-21}$$

Hence, (3-19) and (3-20) can be re-expressed as:

$$a_n = \oint_S ds \left([j\omega\mu_1 \bar{\boldsymbol{\Psi}}_n^4(\mathbf{r}') \cdot \mathbf{n}' \times \mathbf{H}_1(\mathbf{r}')] - [(\nabla' \times \bar{\boldsymbol{\Psi}}_n^4(\mathbf{r}')) \cdot \mathbf{n}' \times \mathbf{E}_1(\mathbf{r}') \right. \tag{3-22}$$

$$0 = \oint_S ds \left([j\omega\mu_2 \bar{\boldsymbol{\Psi}}_n^1(\mathbf{r}') \cdot \mathbf{n}' \times \mathbf{H}_2(\mathbf{r}')] - [(\nabla' \times \bar{\boldsymbol{\Psi}}_n^1(\mathbf{r}')) \cdot \mathbf{n}' \times \mathbf{E}_2(\mathbf{r}') \right. \tag{3-23}$$

where a_n is the spherical expansion coefficients for a plane wave given in (3-19). $\mathbf{E}_1$ and $\mathbf{H}_1$ are the electric and magnetic field components of the incident field.

A possible choice to express unknowns in (3-22) and (3-23) will be the use of spherical harmonics.

$$\mathbf{n}' \times \mathbf{E}_2(\mathbf{r}') = \sum_m \alpha_m \, \mathbf{n}' \times \bar{\boldsymbol{\Psi}}_m^1(\mathbf{r}') \tag{3-24}$$

$$j\omega\mu_2 \mathbf{n}' \times \mathbf{H}_2(\mathbf{r}') = \sum_m \beta_m \, \mathbf{n}' \times \nabla \times \bar{\boldsymbol{\Psi}}_m^1(\mathbf{r}') \tag{3-25}$$

Proof of $\alpha_m = \beta_m$ is given in [30].

Substituting (3-24) and (3-25) in (3-22) and (3-23) yields,

$$a_n = j \sum_m \alpha_m Q_{nm} \tag{3-26}$$

$$Q_{nm} = k_1 \oint_S ds' \left(\frac{\mu_1}{\mu_2} \right) \mathbf{n}' \cdot \nabla' \times \bar{\boldsymbol{\Psi}}_m^1(\mathbf{r}') \times \bar{\boldsymbol{\Psi}}_n^4(\mathbf{r}') - \mathbf{n}' \cdot \bar{\boldsymbol{\Psi}}_m^1(\mathbf{r}') \times \nabla' \times \bar{\boldsymbol{\Psi}}_n^4(\mathbf{r}') \tag{3-27}$$

3.4 T-matrix Formulation

Incident fields can be expanded in terms of vector spherical wave functions and coefficients can be expressed as a_n. Using (3-26), we can obtain α_m and surface unknowns are solved. Hence, we can determine the fields everywhere in space. Using (3-15), scattered fields $\boldsymbol{\phi}_{sca}$ can be calculated using the vector spherical wave functions.

$$\boldsymbol{\phi}_{\text{sca}} = \sum_{n} \mathrm{f_n} \bar{\boldsymbol{\Psi}}_{\mathrm{n}}^{4}(\mathbf{r}) \tag{3-28}$$

In [30] scattering coefficients $\mathrm{f_n}$ are given as,

$$\mathrm{f_n} = -\mathrm{j} \sum_{m} \alpha_{\mathrm{m}} \mathrm{Rg}(\mathrm{Q_{nm}}) \tag{3-29}$$

where $\mathrm{Rg}(\mathrm{Q_{nm}})$ denotes the regular part of $\mathrm{Q_{nm}}$. Hence, we obtain required equation set in order to solve scattering problem with given incident fields. Representing (3-26) and (3-29) as matrix equation gives,

$$\mathbf{a} = \mathrm{j}\bar{\mathbf{Q}} \cdot \boldsymbol{\alpha} \tag{3-30}$$

$$\mathbf{f} = -\mathrm{j}\mathrm{Re}(\bar{\mathbf{Q}}) \cdot \boldsymbol{\alpha} \tag{3-31}$$

$$\mathbf{f} = -\mathrm{Re}(\bar{\mathbf{Q}}) \cdot \bar{\mathbf{Q}}^{-1} \cdot \mathbf{a} \tag{3-32}$$

$$\mathbf{f} = \bar{\mathbf{T}}\mathbf{a} \tag{3-33}$$

$\mathbf{a}, \mathbf{f}, \mathbf{Q}$ and $\boldsymbol{\alpha}$ are the matrix representations of the $\mathrm{a_n}, \mathrm{f_n}, \mathrm{Q_{nm}}$, and α_{m}. Hence, by using (3-33) for a specific scatterer, just by knowing the incident fields, one can find scattered field using its T-matrix.

In order to use T-Matrix formulation we should properly define the incoming and outgoing fields in terms of the basis functions where spherical vector wave functions are used in our case.

In the presence of *N* scatterers we can write the total field as:

$$\mathbf{E}_{\text{total}}(\mathbf{r}) = \mathbf{E}_{\text{incident}}(\mathbf{r}) + \mathbf{E}_{\text{scattered}}(\mathbf{r}) \tag{3-34}$$

$$\mathbf{E}_{\text{total}}(\mathbf{r}) = \bar{\boldsymbol{\Psi}}_{\text{L}}^{1}(\mathbf{r_s}) \cdot \mathbf{a}^{\text{inc}} + \sum_{\text{i}=1}^{N} \bar{\boldsymbol{\Psi}}_{\text{L}}^{4}(\mathbf{r_i}) \cdot \mathbf{b}^{\text{i}} \tag{3-35}$$

where first term on the right side stands for the incoming plane wave and second term is for the scattered field due to *N* scatterers present in the medium. $\mathbf{a}^{\text{inc}}$ is the matrix representation of coefficients of the incoming fields and $\mathbf{b}^{\text{i}}$ is the matrix representation of coefficients of the field scattered by the i^{th} scatterer. Our aim is to determine the $\mathbf{b}^{\text{i}}$ coefficients. In order to find *N* unknown $\mathbf{b}^{\text{i}}$ coefficients, we have to construct *N* linearly independent equations. In the coordinate frame of each scatterer we can use the boundary condition of the scatterer to form *N* linearly independent equations.

For the j^{th} element, we should translate the fields to the j^{th} coordinate frame. Using the addition theorem to translate the multipole coefficients:

$$\bar{\boldsymbol{\Psi}}_{\text{L}}^{1}(\mathbf{r_s}) \cdot \mathbf{a}^{\text{inc}} = \bar{\boldsymbol{\Psi}}_{\text{L}}^{1}(\mathbf{r_j}) \cdot \bar{\beta}(\mathbf{r_{js}}) \cdot \mathbf{a}^{\text{inc}} \tag{3-36}$$

and for $\text{i} \neq \text{j}$

$$\bar{\boldsymbol{\Psi}}_{\text{L}}^{4}(\mathbf{r_i}) \cdot \mathbf{b}^{\text{i}} = \bar{\boldsymbol{\Psi}}_{\text{L}}^{1}(\mathbf{r_j}) \cdot \bar{\alpha}(\mathbf{r_{ji}}) \cdot \mathbf{b}^{\text{i}} \tag{3-37}$$

where $\boldsymbol{\alpha}(\mathbf{r}_{\text{ji}})$ and $\boldsymbol{\beta}(\mathbf{r}_{\text{js}})$ coefficients stand for the translation coefficients in matrix form. Total field for j^{th} element can be expressed as:

$$\begin{aligned}\mathbf{E}_{\text{total}}(\mathbf{r}_{\text{j}}) = \bar{\boldsymbol{\Psi}}_{\text{L}}^{1}(\mathbf{r}_{\text{j}}) \cdot \boldsymbol{\beta}(\mathbf{r}_{\text{js}}) \cdot \mathbf{a}^{\text{inc}} \\ + \sum_{\text{i}=1,\text{i}\neq\text{j}}^{\text{N}} \bar{\boldsymbol{\Psi}}_{\text{L}}^{4}(\mathbf{r}_{\text{i}}) \cdot \boldsymbol{\alpha}(\mathbf{r}_{\text{ji}}) \cdot \mathbf{b}^{\text{i}} + \bar{\boldsymbol{\Psi}}_{\text{L}}^{4}(\mathbf{r}_{\text{j}}) \cdot \mathbf{b}^{\text{j}}\end{aligned} \tag{3-38}$$

First two terms represent the field incident on the j^{th} scatterer and third term denotes the fields scattered by the j^{th} scatterer. Since, third term represents radiating

fields, z_n^4 is to satisfy the radiating boundary conditions. We can relate the incoming fields to the outgoing fields using the T-matrix.

$$\mathbf{b}^j = \overline{\mathbf{T}} \cdot (\boldsymbol{\beta}(\mathbf{r}_{js}) \cdot \mathbf{a}^{inc} + \sum_{i=1,i\neq j}^{N} \bar{\alpha}(\mathbf{r}_{ji}) \cdot \mathbf{b}^i) \tag{3-39}$$

Rearranging the terms:

$$\mathbf{b}^j - \overline{\mathbf{T}} \cdot \sum_{i=1,i\neq j}^{N} \boldsymbol{\alpha}(\mathbf{r}_{ji}) \cdot \mathbf{b}^i = \overline{\mathbf{T}} \cdot \boldsymbol{\beta}(\mathbf{r}_{js}) \cdot \mathbf{a}^{inc} \tag{3-40}$$

If we repeat this procedure for each of the scatterers, we will obtain the required number of independent equations.

3.4.1 T-Matrix Coefficients

Using the boundary conditions on a dielectric sphere we can easily generate the necessary T-matrix coefficients. Since, scattering object is a sphere; T-matrix will be a diagonal matrix.

$$\mathbf{E}_{inc}(\mathbf{r}) = \sum_{n=1}^{\infty} A_{n,m}\mathbf{M}_{n,m}^1 + B_{n,m}\mathbf{N}_{n,m}^1 \tag{3-41}$$

$$\mathbf{E}_{scattered}(\mathbf{r}) = \sum_{n=1}^{\infty} C_{n,m}\mathbf{M}_{n,m}^4 + D_{n,m}\mathbf{N}_{n,m}^4 \tag{3-42}$$

$$\mathbf{E}_{trans}(\mathbf{r}) = \sum_{n=1}^{\infty} E_{n,m}\mathbf{M}_{n,m}^1 + F_{n,m}\mathbf{N}_{n,m}^1 \tag{3-43}$$

Since boundary conditions on a dielectric sphere with a radius of r are given as:

$$\bar{n} \times (\mathbf{E}_{inc} + \mathbf{E}_{scattered}) = \bar{n} \times \mathbf{E}_{transmitted} \tag{3-44}$$

$$\bar{n} \times (\mathbf{H}_{inc} + \mathbf{H}_{scattered}) = \bar{n} \times \mathbf{H}_{transmitted} \tag{3-45}$$

Substituting the multipole terms in equations (3-44) and (3-45), we will obtain 4 independent equations [31]. Since time convention used in reference is different than used in here, there are slight modifications in equations:

$$z_n^1(k_2 r) + c_n z_n^4(k_2 r) = e_n z_n^1(k_1 r) \tag{3-46}$$

$$\frac{k_2}{\mu_2} z_n^1(k_2 r) + \frac{k_2}{\mu_2} d_n z_n^4(k_2 r) = \frac{k_1}{\mu_1} f_n z_n^1(k_1 r) \tag{3-47}$$

$$\begin{aligned} \frac{1}{k_2}\frac{\partial}{\partial r}(r.\, z_n^1(k_2 r)) + \frac{1}{k_2} d_n \frac{\partial}{\partial r}(r.\, z_n^4(k_2 r)) \\ = \frac{1}{k_1} f_n \frac{\partial}{\partial r}(r.\, z_n^1(k_1 r)) \end{aligned} \tag{3-48}$$

$$\begin{aligned} \frac{1}{\mu_2}\frac{\partial}{\partial r}(r.\, z_n^1(k_2 r)) + \frac{1}{\mu_2} c_n \frac{\partial}{\partial r}(r.\, z_n^4(k_2 r)) \\ = \frac{1}{\mu_1} e_n \frac{\partial}{\partial r}(r.\, z_n^1(k_1 r)) \end{aligned} \tag{3-49}$$

Solution of these four equations yield:

$$a_n = -\left. \frac{\mu_1 z_n^1(k_1 r)\frac{\partial}{\partial r}(r.\, z_n^1(k_2 r)) - \mu_2 z_n^1(k_2 r)\frac{\partial}{\partial r}(r.\, z_n^1(k_1 r))}{\mu_1 z_n^1(k_1 r)\frac{\partial}{\partial r}(r.\, z_n^4(k_2 r)) - \mu_2 z_n^4(k_2 r)\frac{\partial}{\partial r}(r.\, z_n^1(k_1 r))} \right|_{r=a} \tag{3-50}$$

$$b_n = -\left. \frac{\mu_1 z_n^1(k_2 r)\frac{\partial}{\partial r}(r.\, z_n^1(k_1 r)) - \mu_2 (\frac{k_1}{k_2})^2 z_n^1(k_1 r)\frac{\partial}{\partial r}(r.\, z_n^1(k_2 r))}{\mu_1 z_n^4(k_2 r)\frac{\partial}{\partial r}(r.\, z_n^1(k_1 r)) - \mu_2 (\frac{k_1}{k_2})^2 z_n^1(k_1 r)\frac{\partial}{\partial r}(r.\, z_n^4(k_2 r))} \right|_{r=a} \tag{3-51}$$

where k_2, ϵ_2 and, μ_2 are constitutive parameters of free space and k_1, ϵ_1 and, μ_1 are constitutive parameters of dielectric sphere of radius a. Using (3-44) and (3-45) one can obtain the scattered field coefficients $C_{n,m}$ and $D_{n,m}$.

$$C_{n,m} = a_n A_{n,m} \tag{3-52}$$

$$D_{n,m} = b_n B_{n,m} \tag{3-53}$$

3.4.2 Iterative Methods

Matrix equation given in (3-40) contains *N* particles and $2(p+1)^2$ unknowns for each particle where p is the truncation number of scattered multipole coefficients. Total number of unknowns is $2N(p+1)^2$ for this problem. To be able to store $(\mathbf{I} - \mathbf{T} \cdot \boldsymbol{\alpha})$, required memory is $O(N^2p^4)$. With several thousand particles, resources of an ordinary computer are inadequate. Also, computational complexity of the Gaussian elimination is $O(N^3p^6)$ floating point operations(flops).

Iterative methods generate a sequence that approximates to the solution of a linear system with reducing error at each successive step. Direct methods generate the exact solution with predefined number of steps by generating the matrix inverse, whereas iterative methods start with an initial guess to the solution and continues till any one of the termination criteria is met.

Main stationary iterative methods are Jacobi, Gauss-Seidel, successive overrelaxation and symmetric successive overrelaxation methods. These methods perform same matrix operations at each step so they are called stationary. However, these methods converge for limited class of matrices.

Non-stationary methods provide better convergencecompared to stationary methods. They converge to the exact solution in *N* steps, however converge (within a

specified tolerance) is usually achieved in a few steps depending on the spectrum of the coefficient matrix.

Conjugate gradient method is an elementary non-stationary method. Several variants like biconjugate gradient and generalized minimal residual methods are presented in literature [32], [33]. Due to its simplicity and convergence for non-symmetric matrices, biconjugate gradient stabilized (BICGSTAB) method is commonly used. Details of the algorithm will not be provided here since it is an easily accessible algorithm [32]. In literature different algorithms have also been proposed like preconditioned GMRES [34]. Despite the fact that preconditioning and alternative solvers may improve the performance of FMM solvers, they are not used in the present work and left as a future work.

BICGSTAB algorithm is provided below [32]:

1. Compute $r_0 \coloneqq b - Ax_0$; r_0' arbitrarily selected.
2. $p_0 \coloneqq r_0$
3. $for\ j = 0,1, \ldots until\ convergence\ Do$:
4. $\alpha_j \coloneqq (r_j, r_0')/(Ap_j, r_0')$
5. $s_j \coloneqq r_j - \alpha_j Ap_j$
6. $w_j \coloneqq (As_j, s_j)/(As_j, As_j)$
7. $x_{j+1} \coloneqq x_j + \alpha_j p_j + w_j s_j$
8. $r_{j+1} \coloneqq s_j - w_j As_j$
9. $\beta_j \coloneqq \frac{(r_{j+1}, r_0')}{(r_j, r_0')} . \frac{\alpha_j}{w_j}$
10. $p_{j+1} \coloneqq r_{j+1} + \beta_j (p_j - \omega_j Ap_j)$
11. $End\ Do$

The procedure is repeated till the norm of the residuals calculated in the 8th step drops below a certain threshold.

CHAPTER 4

DIAGONALIZATION OF THE VECTOR ADDITION THEOREM

4.1 Introduction

FMM (Fast Multipole Method) method was invented by Rokhlin and Greengard [25] and announced as one of the best ten algorithms of 20^{th} century [26]. FMM is developed for the fast summation of the multipole solution of Laplace equation and reduces the computation time of matrix-vector products of a solver. Elements are grouped and interactions between the electrically far groups are treated as if they were a single scatterer. Thus, space should be divided into two groups, which are called near and far groups. Hence, instead of computing the pairwise interaction, interactions between the groups are analyzed. Therefore, due to the N elements computational work during the calculation of the interactions is N instead of N^2. Treating a group of a scatterer as a single scatterer also reduces the memory requirement significantly, since interaction matrix between the elements is not explicitly formed.

Assume that we have N elements grouped within a sphere. Using addition theorem, total scattered fields can be represented as summation of vector spherical wave functions expressed in a coordinate frame having its origin at the center of this sphere. Consider another sphere where M elements are located in it. In order to calculate interactions between the elements of two spheres, we have to carry out O(NM) operations. Instead of calculating the pairwise interactions directly, multipole coefficients of the total field due to N spheres expressed in a coordinate frame centered at first sphere can be translated to the elements of the second sphere.

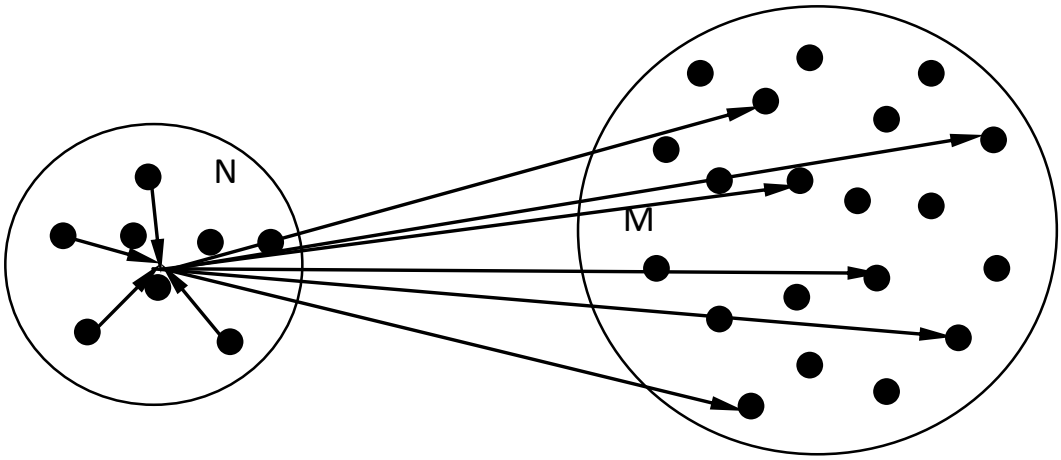

Figure 4.1 Field scattered from each element shown of *N* is translated to group's center and then interactions with elements of *M* are calculated from the center of *N* once. Hence, interaction count between groups of elements could be reduced with the use of multipole elements. (Only several interactions are demonstrated due to clarity)

Then, for translating multipoles of the first sphere we have to carry out $N(p+1)^2$ operations, where $(p+1)^2$ denotes the number of multipoles and p denotes truncation number. Then, interaction between the $(p+1)^2$ multipoles of each of the *M* elements can be calculated in $M(p+1)^2$ operations. Hence, total operation count is $(N+M)(p+1)^2$. For *N* and *M* larger than $(p+1)^2$ we have an advantage compared to the direct algorithm.

Assume that we have two groups of scatterers with *N* and *M* elements as shown in Figure 4.1. In the following, we will name the groups by their element numbers. We first translate the outgoing multipole coefficients of each scatterer to the center of the group as shown in Figure 4.1. By summing up the translated coefficients we obtain the multipole expansion of the group and this step is called aggregation. Therefore, only $(p+1)^2$ multipoles are available at the center, independent of element count of *N*. In Figure 4.1 interactions are calculated directly after this step. However, when there are many groups as shown in Figure 4.2, it will be wiser to translate multipoles centered at group *N* to the center of each group denoted by *M*. This step is called translation since multipoles are translated from one group center to another. Final step is called disaggregation. In this step, multipoles

translated to the center of the groups *M* are distributed again on to the particles in the same group. Hence, particle to particle interaction is computed in three steps.

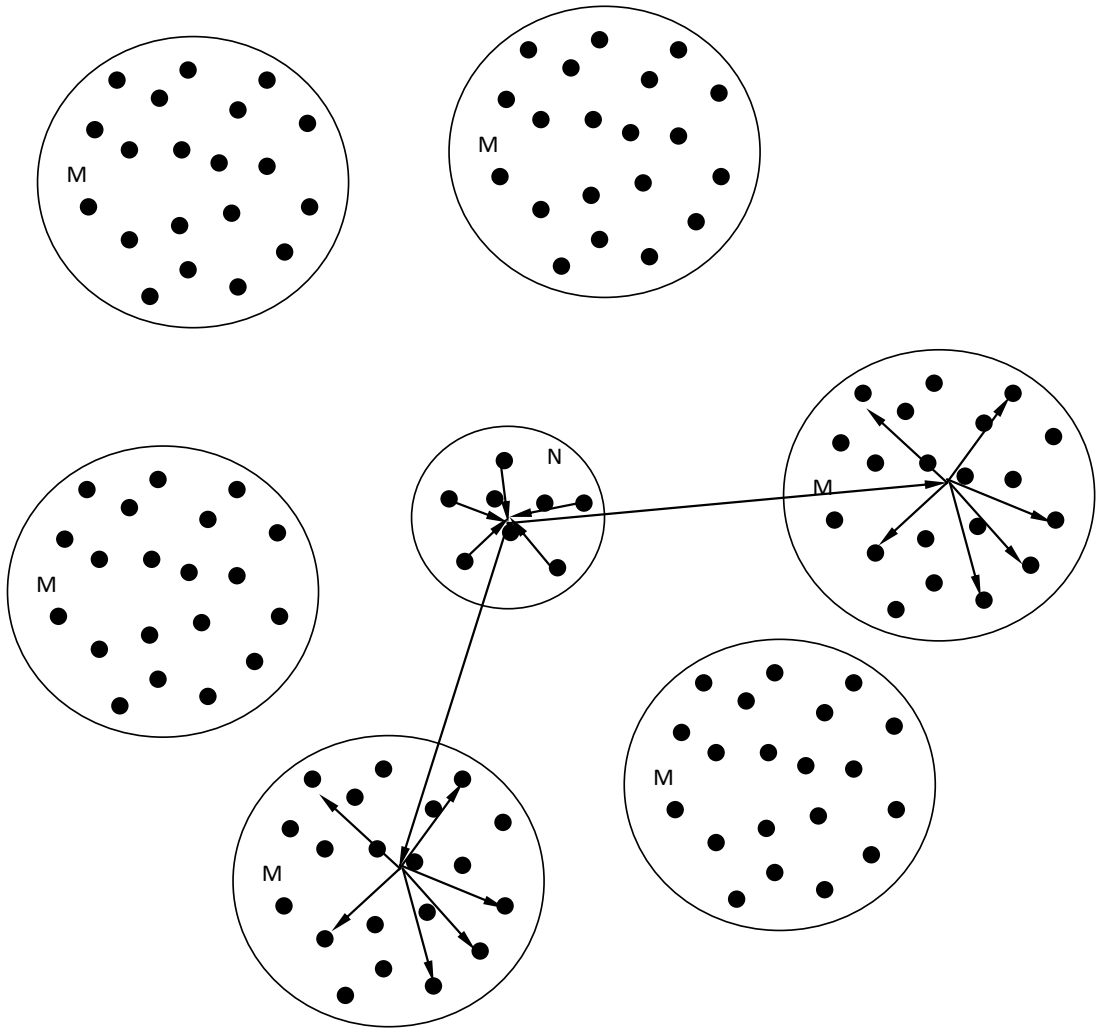

Figure 4.2 Calculation of particle interaction amongst particle located in *N* and particles distributed in space and demonstrated with *M*. (Only several interactions are demonstrated due to clarity)

The advantage of describing the algorithm in three steps, namely, aggregation, translation and disaggregation steps can be more easily explained, if we consider the distribution of particles shown in Figure 4.3. Particles are first grouped according to their location as shown in the figure. Near elements are collected in a group. Fields outgoing from each group are aggregated to group center. Then aggregated fields are translated to the other groups.

When we consider a single group as shown in the right bottom corner of Figure 4.3, aggregated fields are translated to the center of this group (Demonstrated with long arrows). Then, all translated fields are summed. The result is an expression of the field scattered by all such groups at the center of this particular group.

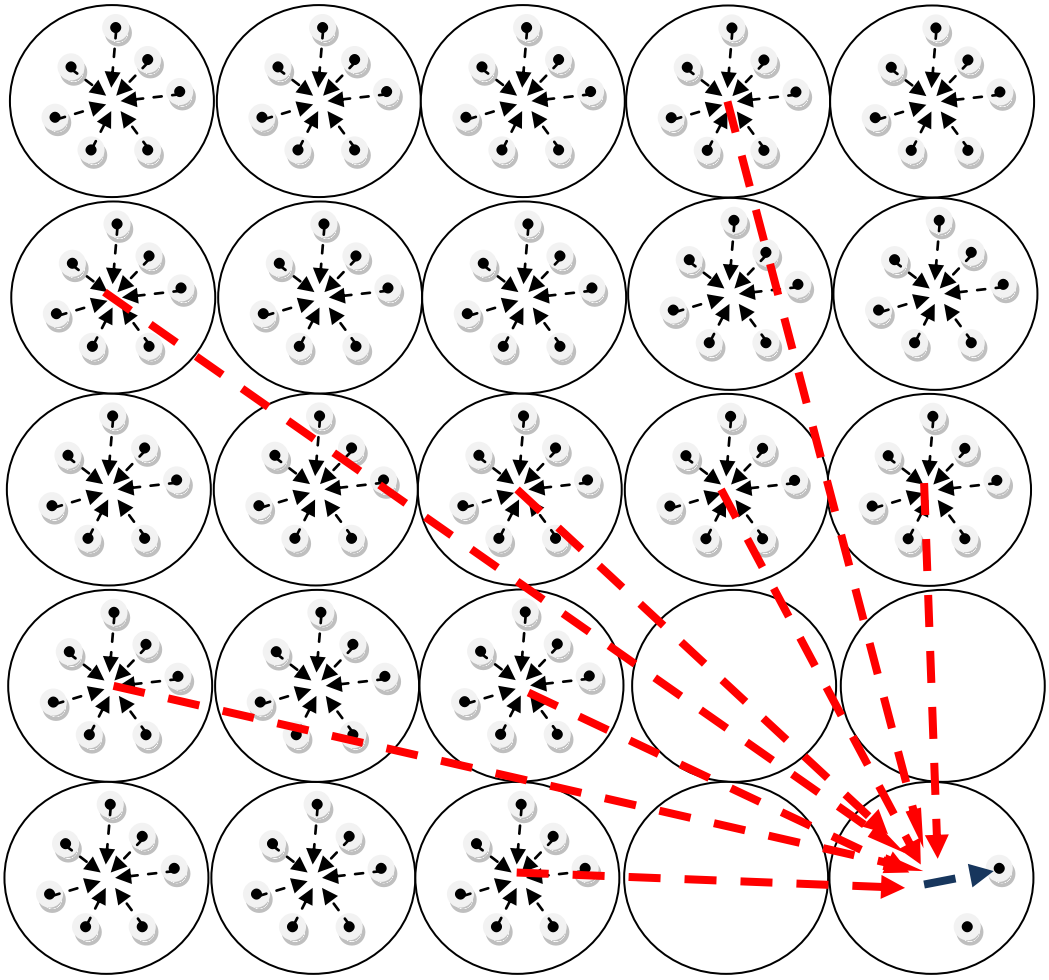

Figure 4.3 Computational space is divided into groups. Scattered fields in each group are translated to group center. From the far groups, aggregated fields are translated to target groups one by one (long vectors). At disaggregation step, summation of translated fields is translated to particle location of target group.

Final step is disaggregation. Fields at the center of the sphere has to be translated to the center of each scatterer. If the size of the scatterers in each group is of the same order, the same number of multipole coefficients, i.e., only $(p+1)^2$ multipole coefficients will be enough for T-matrix formulations. Hence, all of the far field interactions are completed.

Due to convergence problems in vector addition theorem, some of the interactions should be omitted in these three steps. If the norm of the vector used for aggregation and disaggregation is equal to or bigger than the vector used for translation, then vector addition theorem fails. For such scatterers, interactions between the elements should be calculated using the traditional methods. In Figure 4.3, aggregation step of the touching spheres are not shown intentionally, since vector addition theorem cannot be applied in neighboring groups. Particle interactions in these groups should be calculated directly.

4.2 Diagonalization of the Spherical Translation Operators

Procedure given in section 4.1 is required for the acceleration of the pairwise interactions. However, this method still can be improved with the diagonalization of the translation operator. Hence, with diagonalization, faster algorithms can be implemented.

During the calculation of the pair wise interactions of the scatterers, we have to compute the expression in equation (3-37), where L is a shorthand notation for n,m.

$$\bar{\boldsymbol{\Psi}}_{\mathrm{L}}^{4}(\mathbf{r}_{\mathrm{i}}) = \bar{\boldsymbol{\Psi}}_{\mathrm{L}}^{1}(\mathbf{r}_{\mathrm{j}}) \cdot \boldsymbol{\alpha}(\mathbf{r}_{\mathrm{ji}}) \tag{4-1}$$

Instead of translating the multipole coefficients in single operation, we can perform the translation of the coordinate frame in three steps. Hence, instead of computing $\boldsymbol{\alpha}(\mathbf{r}_{\mathrm{ji}})$ which is the matrix representation of the translation coefficients, we compute three translation coefficients where

$$\boldsymbol{\alpha}(\mathbf{r}_{\mathrm{ji}}) = \boldsymbol{\beta}(\mathbf{r}_{\mathrm{j}\lambda'})\boldsymbol{\alpha}(\mathbf{r}_{\lambda'\lambda})\boldsymbol{\beta}(\mathbf{r}_{\lambda\mathrm{i}}) \tag{4-2}$$

Then we can re-express equation (3-40) as:

$$\mathbf{b}^{j} - \overline{\mathrm{T}} \cdot \left[\sum_{\ell \in N, i \in G, i \neq j} \boldsymbol{\alpha}(\mathbf{r}_{ji}) \cdot \mathbf{b}^{i} + \sum_{\ell \notin N, i \in G} \sum \alpha(\mathbf{r}_{ji}) \cdot \mathbf{b}^{i} \right] = \overline{\mathrm{T}} \cdot \boldsymbol{\beta}(\mathbf{r}_{js}) \cdot \mathbf{a}^{inc} \tag{4-3}$$

Scatterers are divided into groups. ℓ shows the number of the group and N stores the neighbouring groups of ℓ and ℓ itself. G stands for the elements in the group ℓ. Hence, first sum shows the near field interactions and second sum is for the far field interactions where FMM will be used.

4.3 Diagonalization of Vector Addition Theorem

Vector addition theorem is presented in the second chapter. In this section, the diagonalization of the vector addition theorem is described [35]. This diagonalization of the vector addition theorem and its application to scattering problems is the core of this thesis.

According to [35], plane wave can be expanded as, where L is a shorthand for (l,m):

$$\boldsymbol{\kappa} e^{j\mathbf{k}\cdot\mathbf{r}} = \sum_{L} 4\pi j^{l} [\, \mathbf{M}_{L}^{1}(\mathbf{r}) \mathbf{X}_{L}^{*}(\mathbf{k}) + \mathbf{N}_{L}^{1}(\mathbf{r}) \mathbf{Y}_{L}^{*}(\mathbf{k})] \cdot \boldsymbol{\kappa} \tag{4-4}$$

$\boldsymbol{\kappa}$ is a 3x3 diadic, whose first two components can be found by adding $\pi/2$ to the θ and ϕ of $\mathbf{k}$ respectively. Third component is simply the 0 vector. Hence $\boldsymbol{\kappa} \cdot \mathbf{k} = 0$ (In [35] definition of $\boldsymbol{\kappa}$ is inadequate)

Definitions of the operators and functions are given below:

$$\mathbf{X}_{L}(\mathbf{r}) = \frac{\mathbf{L} Y_{n,-m}(\theta, \phi)}{\sqrt{l(l+1)}} \tag{4-5}$$

$$\mathbf{Y}_{L}(\mathbf{r}) = j\mathbf{r} \times \mathbf{X}_{L}(\mathbf{r}) \tag{4-6}$$

where the **L** operator is defined as:

$$\mathbf{L} = \frac{1}{\mathrm{j}}\mathbf{r} \times \nabla \tag{4-7}$$

Define a new variable:

$$\mathbf{W}_{\mathrm{L}}(\mathbf{k}) = [\mathbf{X}_{\mathrm{L}}(\mathbf{k}) \quad \mathbf{Y}_{\mathrm{L}}(\mathbf{k})] \tag{4-8}$$

Then equation (4-4) can be written as:

$$\mathbf{I}e^{\mathrm{j}\mathbf{k}\cdot\mathbf{r}} = \sum_{\mathrm{L}} 4\pi \mathrm{j}^{\mathrm{l}}\, \bar{\boldsymbol{\Psi}}^{1}_{\mathrm{L}}(\mathbf{r}) \cdot \mathbf{W}^{*}_{\mathrm{L}}(\mathbf{k}) \tag{4-9}$$

Using these expressions, plane wave expansion of $\bar{\boldsymbol{\Psi}}^{1}_{\mathrm{L}}$ can be written as an integral over a unit sphere:

$$\bar{\boldsymbol{\Psi}}^{1}_{\mathrm{L}}(\mathbf{r}) = \frac{1}{4\pi \mathrm{j}^{\mathrm{l}}} \oint \mathbf{I} \cdot \mathbf{W}_{\mathrm{L}}(\mathbf{k}) e^{\mathrm{j}\mathbf{k}\cdot\mathbf{r}} d\hat{\mathrm{k}} \tag{4-10}$$

Using the scalar addition theorem to expand $e^{\mathrm{j}\mathbf{k}\cdot\mathbf{r}}$:

$$e^{\mathrm{j}\mathbf{k}\cdot\mathbf{r}_2} = \sum_{\mathrm{L}''} 4\pi \mathrm{j}^{\mathrm{l}''}\, \varphi^{1}_{\mathrm{L}''}(\mathbf{k}) \mathrm{Y}^{*}_{\mathrm{L}''}(\mathbf{k}) \tag{4-11}$$

Since

$$\mathbf{I}e^{\mathrm{j}\mathbf{k}\cdot\mathbf{r}} = \mathbf{I}e^{\mathrm{j}\mathbf{k}\cdot\mathbf{r}_1} \cdot e^{\mathrm{j}\mathbf{k}.\mathbf{r}_2} \tag{4-12}$$

where $\mathbf{r} = \mathbf{r}_1 + \mathbf{r}_2$. Substituting (4-9) and (4-11) into (4-10) we obtain:

$$\bar{\boldsymbol{\Psi}}^{1}_{\mathrm{L}}(\mathbf{r}) = \frac{1}{4\pi \mathrm{j}^{\mathrm{l}}} \sum_{\mathrm{L}'} 4\pi \mathrm{j}^{\mathrm{l}'} \bar{\boldsymbol{\Psi}}^{1}_{\mathrm{L}'}(\mathbf{r}_1) \cdot \beta_{\mathrm{L}',\mathrm{L}}(\mathbf{r}_2) \tag{4-13}$$

$$\beta_{\mathrm{L}',\mathrm{L}}(\mathbf{r}_2) = \sum_{\mathrm{L}''} 4\pi \mathrm{j}^{\mathrm{l}'+\mathrm{l}''-\mathrm{l}} \varphi^{1}_{\mathrm{L}''}(\mathbf{r}_2) \cdot \bar{\mathrm{A}}_{\mathrm{L},\mathrm{L}',\mathrm{L}''} \tag{4-14}$$

$$\overline{A}_{L,L',L''} = \oint \mathbf{W}^*_{L'} \mathbf{W}_L(\mathbf{k}) Y^*_{L''}(\mathbf{k}) d\hat{k} \tag{4-15}$$

where integration is over an unit sphere and $\beta_{L',L}$ is the translation coefficients of the vector addition theorem.

Different forms of vector addition theorem can be generated similarly. As given in equation (4-14), where β is the regular part of the α, α coefficients can be obtained by:

$$\alpha_{L',L}(\mathbf{r}_2) = \sum_{L''} 4\pi j^{l'+l''-l} \varphi^4_{L''}(\mathbf{r}_2) \cdot \overline{A}_{L,L',L''} \tag{4-16}$$

Hence we have three sets of equations

$$\bar{\boldsymbol{\Psi}}^1_L(\mathbf{r}) = \frac{1}{4\pi j^l} \sum_{L'} 4\pi j^{l'} \bar{\boldsymbol{\Psi}}^1_{L'}(\mathbf{r}_1) \cdot \beta_{L',L}(\mathbf{r}_2) \tag{4-17}$$

$$\bar{\boldsymbol{\Psi}}^4_L(\mathbf{r}) = \frac{1}{4\pi j^l} \sum_{L'} 4\pi j^{l'} \bar{\boldsymbol{\Psi}}^1_{L'}(\mathbf{r}_1) \cdot \alpha_{L',L}(\mathbf{r}_2) \;\; |\mathbf{r}_1| < |\mathbf{r}_2| \tag{4-18}$$

$$\bar{\boldsymbol{\Psi}}^4_L(\mathbf{r}) = \frac{1}{4\pi j^l} \sum_{L'} 4\pi j^{l'} \bar{\boldsymbol{\Psi}}^4_{L'}(\mathbf{r}_1) \cdot \beta_{L',L}(\mathbf{r}_2) \;\; |\mathbf{r}_1| > |\mathbf{r}_2| \tag{4-19}$$

4.3.1 An Orthogonality Identity

We know from equation (4-9) that

$$\mathbf{I} e^{j\mathbf{k}\cdot\mathbf{r}} = \sum_{L} 4\pi j^l \, \bar{\boldsymbol{\Psi}}^1_L(\mathbf{r}) \cdot \mathbf{W}^*_L(\mathbf{k}) \tag{4-20}$$

and from equation (4-10)

$$\bar{\boldsymbol{\Psi}}^1_L(\mathbf{r}) = \frac{1}{4\pi j^l} \oint \mathbf{I} \cdot \mathbf{W}_L(\mathbf{k}) e^{j\mathbf{k}\cdot\mathbf{r}} d\hat{k} \tag{4-21}$$

where integration is over unit sphere. Using (4-21) in (4-20)

$$\mathbf{I}e^{j\mathbf{k}\cdot\mathbf{r}} = \oint \mathbf{I}\, e^{j\mathbf{k}'\cdot\mathbf{r}} \sum_{L} \mathbf{W}_L(\mathbf{k}')\mathbf{W}_L^*(\mathbf{k})\, d\hat{k} \tag{4-22}$$

Hence we can say

$$\sum_{L} \mathbf{W}_L(\mathbf{k}')\mathbf{W}_L^*(\mathbf{k}) = \delta(\mathbf{k}' - \mathbf{k})\mathbf{I} \tag{4-23}$$

4.3.2 Diagonalization

Using (4-11) we can rewrite (4-14) as:

$$\beta_{L',L}(\mathbf{r}_2) = j^{l'-l} \oint \mathbf{W}_L(\mathbf{k}')\mathbf{W}_{L'}^*(\mathbf{k})e^{j\mathbf{k}\cdot\mathbf{r}}\, d\hat{k} \tag{4-24}$$

As can be seen in (4-2) α can be expressed in three steps

$$\alpha(\mathbf{r}_{ji}) = \beta(\mathbf{r}_{j\lambda'})\alpha(\mathbf{r}_{\lambda'\lambda})\beta(\mathbf{r}_{\lambda i}) \tag{4-25}$$

Substituting (4-24) in (4-25) and making suitable exchange of operators, we have:

$$\begin{aligned}\alpha_{L,L'}(\mathbf{r}_{ij}) &= \oint \oint d\hat{k}d\hat{k}'\, j^{l}\mathbf{W}_L^*(\mathbf{k})e^{j\mathbf{k}\cdot\mathbf{r}_{i\lambda}} \\ &\sum_{L_1,L_2} j^{l_2-l_1}\mathbf{W}_{L_1}(\mathbf{k})\,\alpha_{L_1,L_2}(\mathbf{r}_{\lambda,\lambda'})\mathbf{W}_{L_2}^*(\mathbf{k}')i^{l'}\mathbf{W}_{L'}(\mathbf{k}')e^{j\mathbf{k}'\cdot\mathbf{r}_{\lambda' j}}\end{aligned} \tag{4-26}$$

We define a new function to replace double summation in (4-26) as:

$$\tilde{\alpha}(\mathbf{r}_{\lambda'\lambda}, \mathbf{k}, \mathbf{k}') = \sum_{L_1,L_2} j^{l_2-l_1}\mathbf{W}_{L_1}(\mathbf{k})\,\alpha_{L_1,L_2}(\mathbf{r}_{\lambda,\lambda'})\mathbf{W}_{L_2}^*(\mathbf{k}') \tag{4-27}$$

which can be simplified to:

$$\begin{aligned}&\alpha_{L_1,L_2}(\mathbf{r}_{\lambda,\lambda'}) \\ &= \sum_{L''} 4\pi j^{l_1+l''-l_2}\varphi_{L''}^4(\mathbf{r}_{\lambda,\lambda'}) \oint d\hat{k''}\, \mathbf{W}_{L_1}^*(\mathbf{k}'')\mathbf{W}_{L_2}(\mathbf{k}'')Y_{L''}^*(\mathbf{k}'')\end{aligned} \tag{4-28}$$

Use (4-28) in (4-27)

$$\tilde{\alpha}(\mathbf{r}_{\lambda'\lambda}, \mathbf{k}, \mathbf{k'}) = \sum_{L''} \varphi^{4}_{L''}(\mathbf{r}_{\lambda,\lambda'}) \oint d\widehat{k''}\, Y^{*}_{L''}(\mathbf{k''}) 4\pi j^{l''} \sum_{L_1,L_2} \mathbf{W}_{L_1}(\mathbf{k})\, \mathbf{W}^{*}_{L_1}(\mathbf{k''}) \mathbf{W}_{L_2}(\mathbf{k''}) \mathbf{W}^{*}_{L_2}(\mathbf{k''}) \tag{4-29}$$

Also using (4-23) we obtain the diagonalized form as

$$\alpha_{L,L'}(\mathbf{r}_{ij}) = \oint d\hat{k}\, \mathbf{W}^{*}_{L}(\mathbf{k}) e^{j\mathbf{k}\cdot\mathbf{r}_{i\lambda}} \tilde{\alpha}(\mathbf{r}_{\lambda'\lambda}, \mathbf{k}, \mathbf{k'}) j^{l'} e^{j\mathbf{k'}\cdot\mathbf{r}_{\lambda'j}} \mathbf{W}_{L'}(\mathbf{k'}) \tag{4-30}$$

and

$$\tilde{\alpha}(\mathbf{r}_{\lambda'\lambda}, \mathbf{k}, \mathbf{k'}) = \mathbf{I} \sum_{L''} \varphi^{4*}_{L''}(\mathbf{r}_{\lambda,\lambda'}) 4\pi j^{l''} Y_{L''}(\mathbf{k}) \tag{4-31}$$

4.4 Error Sources

There are several error sources in the formulation of the scattering problem. Error can be reduced up to some extent. Due to modeling of scatterer volume as cluster of spheres, electromagnetic model in simulator and actual geometry have some discrepancies. Error coming from the discretization of body is minimized with selection of smaller spheres compared to wavelength. All of the particles used for simulations have a diameter of 0.1λ or smaller. For metallic objects, diameters of spheres reduced down to 0.04λ.

Another source of error is coming from the expression given in (2-62). Since it is not possible to extend summations up to infinity, it has to be truncated to a certain value. [34] suggests use of error maps based on solution of a scattering problem, that consists of two scatterers excited with a plane wave. Since solution will be fast just for two scattering elements, construction of such a table will be an easy task. In this work importance of particle radius and particle separation ratio is emphasized. For touching spheres, truncation number increases substantially. Truncation number according to the radius of the spheres are given by [34]:

$$L \approx [ka] + p_0(ka, \varepsilon, \delta) \tag{4-32}$$

Equation given in (4-32) is used for determination of truncation number for a given scatterer. k is the wave number and "a" is the radius of scatterer. p_0 can be found using Figure 4.4. ϵ denotes accuracy of the solution, δ is defined by the ratio of distance between the scatterer center and closest point on surface of nearest scatterer to the radius of the scatterer. Hence δ is equals to one when two scatterers are touching to each other. For our case δ is less than one. Hence, spheres are overlapping. This case is not considered in literature since it is a hypothetical case and does not have a physical counterpart.

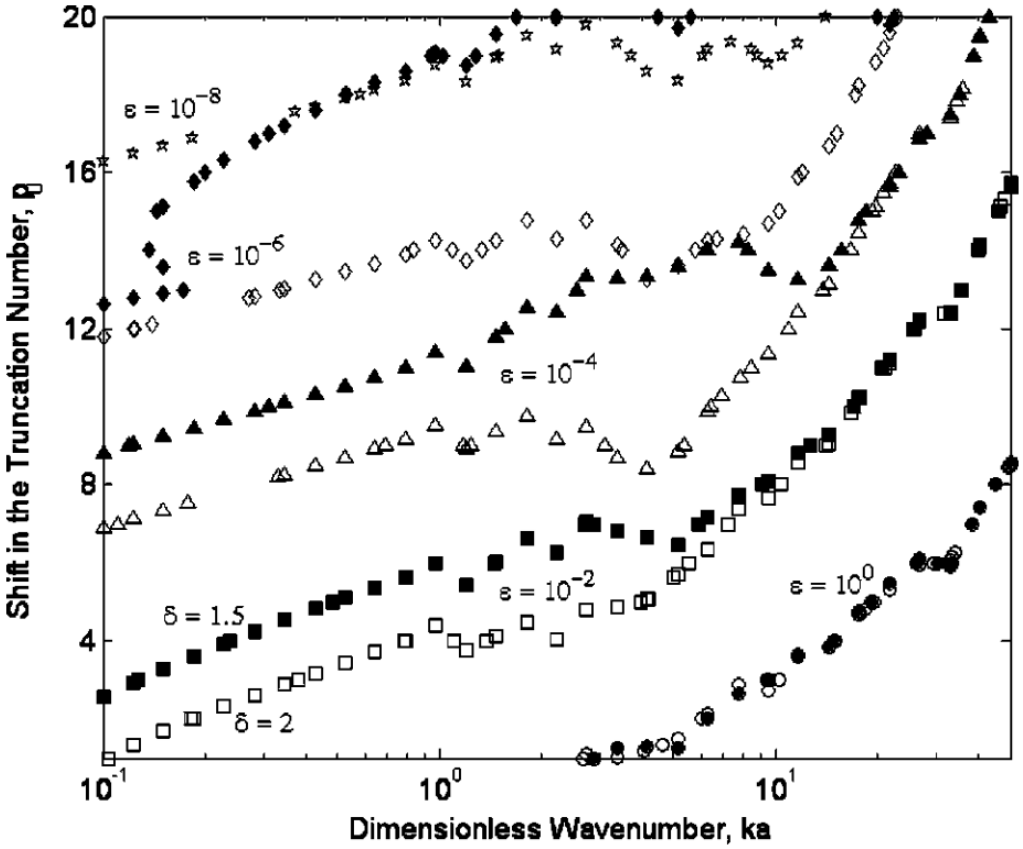

Figure 4.4 According to required accuracy ε and given δ due to distribution of the scatterers required shift p_0 can be found using error maps obtained using scattering calculation of two spheres. Filled markers demonstrates δ=1.5 condition and hollow markers are for δ=2 condition. Objects under consideration are sound hard spheres with equal dimensions. (Figure is obtained from [34])

[36] also addresses the same problem. While the scatterers approach each other, field interaction becomes effective around the contact point. Hence, higher number of terms should be used for the representation of the gradient in field.

However, due to increased number of terms, with densely distributed scatterers and increased number of interacting multipole coefficients, solution time can be dominated by the near field interactions. For such cases, near field interactions could be several orders of magnitude higher than far field interactions. [37] sets truncation number as L″/2, since outgoing fields are rapidly decaying for multipoles with higher orders.

[38] defines FMM as an approximate tool for the evaluation of particle interactions, due to errors in truncation of expansions and numerical integrations. Detailed error analysis is also presented. Truncation number N_α for L'' in (4-31) is bounded due to oscillation characteristics of the Hankel function and given by,

$$N_\alpha < 2kD \tag{4-33}$$

Here, D is the group size. However, it should be high enough for the convergence of the expansion with desired accuracy. In order to have a desired accuracy, an empirical formula for N_α is given in [39] as,

$$N_\alpha \approx ka + 1.8 d_0^{2/3} (ka)^{1/3} \tag{4-34}$$

where $d_0=\log(1/\epsilon)$, the number of digits accuracy and "a" is the radius of scatterers.

At the final stage of the FMM implementation integration given in (4-30) has to be implemented. Since it is not straightforward to implement the integration analytically, numerical techniques are used for the implementation. For the numerical evaluation of the integral quadrature rule is used. Quadrature rule can be implemented as

$$\int_{-1}^{1} f(x)dx \approx \sum_{i=1}^{n} w_i f(x_i) \tag{4-35}$$

Hence, integration of $f(x)$ over the interval [-1,1] can be approximated as weighted sum w_i of the function at specific points x_i. If Gauss quadrature is used, approximation given in (4-35) is exact for polynomials with degrees equals or less than 2n-1. Numerical errors are also investigated in [40] and [41]. Since integral

given in (4-30) is a double integral over θ and ϕ, integral over θ is implemented with N_θ Gauss-Legendre points and integral over ϕ is implemented with equally spaced $2N_\theta$ points over the interval [-π,π]. Weighting functions for ϕ is π/N_θ. Such implementation is exact for harmonics $n<2N_\theta$. Selection of N_θ as

$$N_\theta = N_\alpha + 1 \tag{4-36}$$

will provide exact results with the assumption of

$$N_\alpha > 2L \tag{4-37}$$

With the condition given in (4-36), integration error is below the truncation error, hence it can be ignored and for the error analysis only truncation error can be used [41].

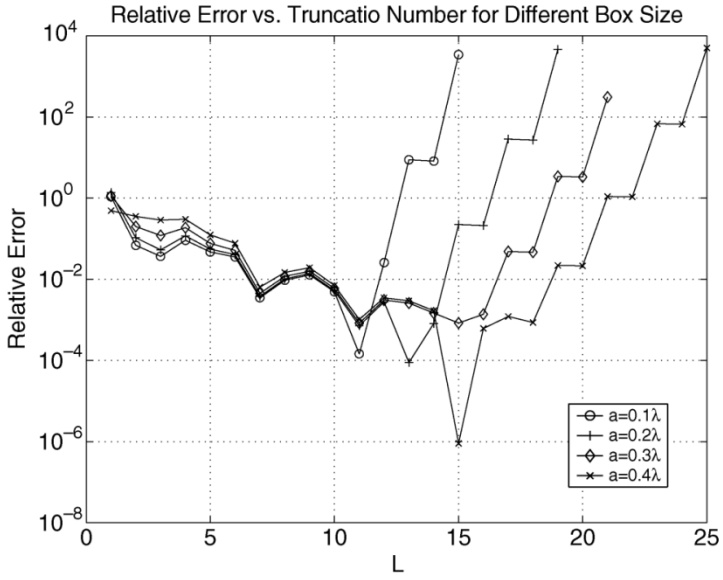

Figure 4.5 Relative error of FMM with respect to truncation number N_α and group size D. [42] proposes the use of FMM for group size larger than 0.2λ due to increased relative error of the translation step. For smaller group sizes low frequency FMM is recommended. (Figure is obtained from [42])

For plane wave based algorithms [42] suggests the minimum of ~0.2λ group size, which is the point of interest due to diagonalization in terms of the plane waves.

Figure 4.5 demonstrates the relative error of the plane wave based FMM algorithm with respect to group size.

As stated by [34] minimum D set by validity of multipole expansions at the surface of the scatterers are given by,

$$D > 3.15a \tag{4-38}$$

Again D is the group size and "a" is the common radius of the scatterers. Due to translation of the expansions, a tighter requirement given by [34] is,

$$D > 3.73a \tag{4-39}$$

4.5 Numerical Results

Using the methods presented in Chapter 2, 3 and 4, we have implemented a FMM solver in MATLAB. MATLAB as a development environment can speed up development process due to readily available algorithms and availability of multidimensional arrays. However, in the subsequent steps, performance of MATLAB degrades due to the increased particle count. Hence, as an alternative to MATLAB, code is implemented in C++. However, since C++ is a low level language, most of the algorithms are not available. Hence, they have to be implemented separately. Since a functional FMM comde has been developed in MATLAB, a similar syntax is preferred. Due to its speed and ease of use, Armadillo Linear Algebra libraries are used in conjunction with the subroutines like Basic Linear Algebra Subprograms (BLAS) and Linear Algebra Package (LAPACK). With some modifications, code is implemented in C++. Speed improvement is drastic. However, code debugging is a time consuming step in C++ development. Armadillo libraries can generate unexpected errors and code has to be implemented with great care. For the initial development stage, one should prefer high level languages. However, for speed improvement, low level languages like C++ or FORTRAN is mandatory.

4.5.1 Scattering Calculations of Dielectric Bodies

For verification purposes, a dielectric sphere is illuminated by a plane wave and back scattering of the object is calculated. Selection of a sphere is useful since scattering from spherical scatterers are investigated in detail and results are widely available [43].

For the investigation of the dielectric scattering case, a dielectric scatterer's normalized radar cross section is evaluated with Mie's series. For comparison, dielectric sphere is meshed with smaller spheres and backscattering is computed using FMM algorithm.

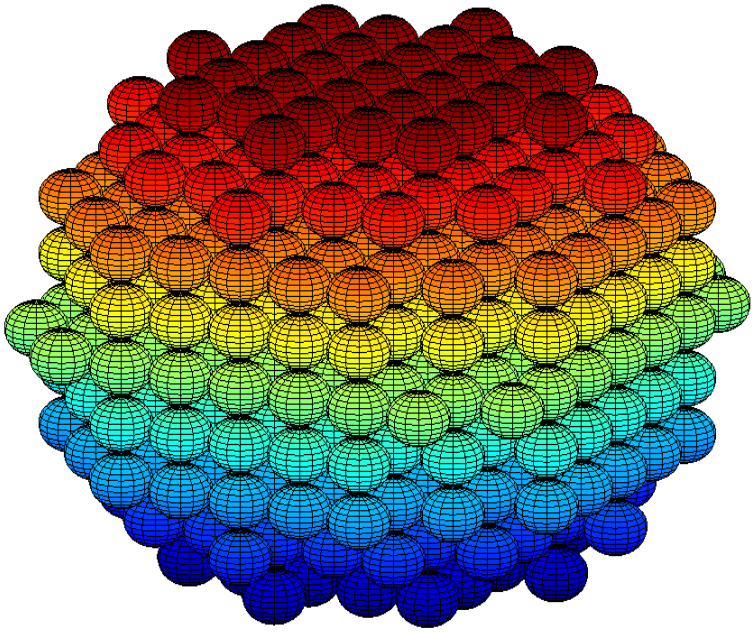

Figure 4.6 Dielectric sphere is represented as cluster of smaller spheres. Each sphere in cluster has same radius. Total volume of the large scattering body is represented with a number of smaller spheres.

Meshing of the dielectric body is implemented along x, y and z coordinate axes. Hence, every scatterer center is located at ($x \cdot \Delta m$, $y \cdot \Delta m$, $z \cdot \Delta m$). Δm is the mesh size of the problem and x, y and z are integer numbers. Also, center of the dielectric

body should be closer than R, to the center of coordinate frame. Volume of each scatterer is selected such that it can represent the volume of a corresponding cube with side length of Δm. Hence, radius of the sphere can be chosen as

$$r = \sqrt[3]{\frac{3}{4\pi}}\Delta m \tag{4-40}$$

Dielectric constants (ε_r) of smaller spheres are selected to be same as the original dielectric sphere. For various dielectric scatterer radii, geometry is meshed and FMM results are compared with Mie series' solution. Figure 4.7 depicts FMM results and Mie series' solution. Horizontal axis denotes simulated spheres' radius. Vertical axis is normalized monostatic radar cross section as defined in [42]. Simulations are in agreement with theoretical results.

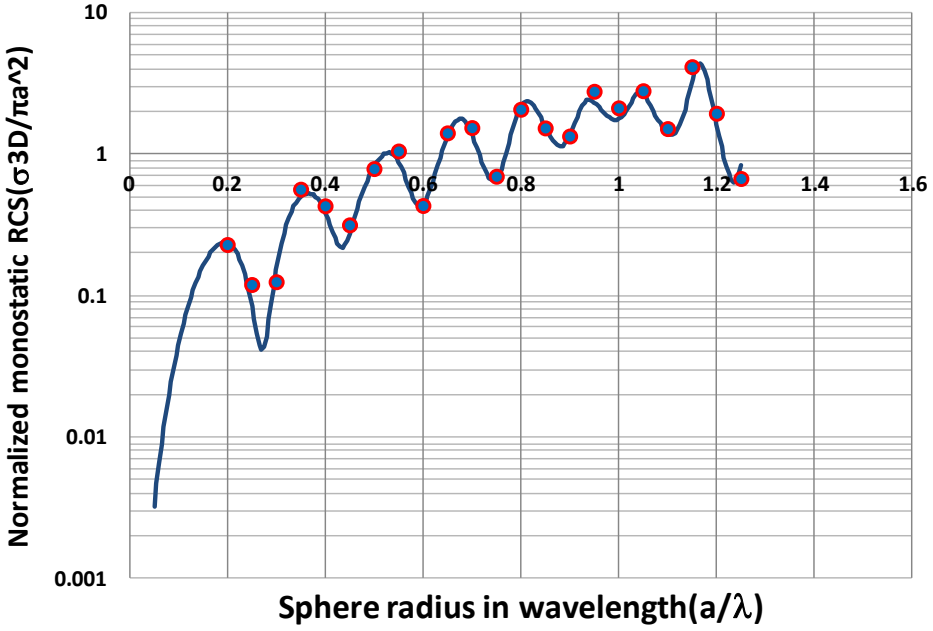

Figure 4.7 For various dielectric scatterer radiuses, normalized monostatic RCS is calculated and compared with Mie series solution. (Dots represent the FMM solver results)

While sphere radius is increasing, number of small spheres that represents the actual sphere also increases. Hence, number of unknowns is increasing with larger dielectric spheres. As can be seen in Figure 4.8, in order to properly represent the original scatterer volume, number of small spheres has to be increased in a cubical

law fashion. Since volume increases with r^3, number of elements increases with $O(r^3)$.

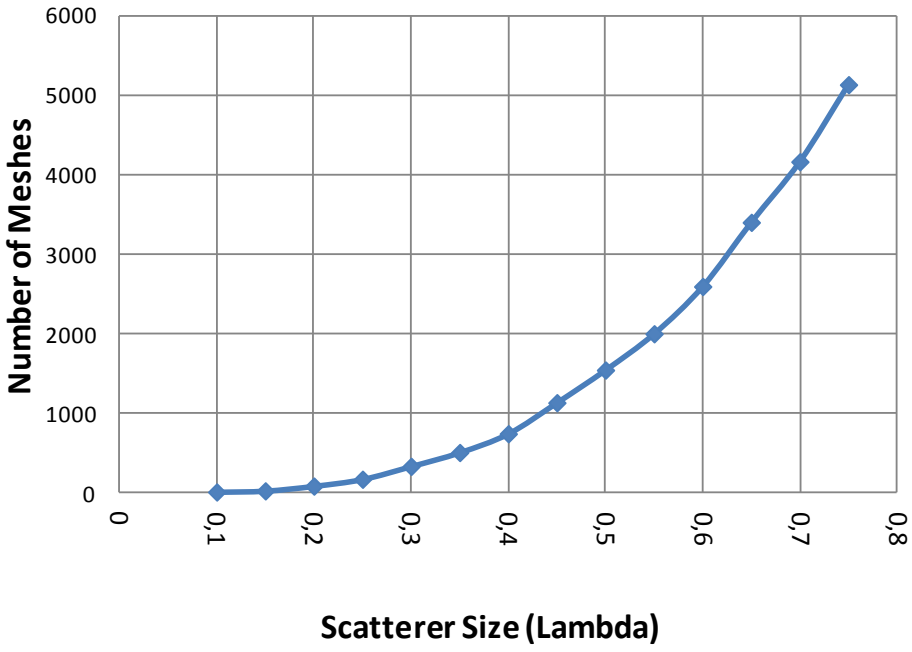

Figure 4.8 In order to represent dielectric sphere with increasing radius, number of particles should also enhanced. Mesh size is kept constant with increasing dielectric scatterer size. Hence due to $O(r^3)$ increase in volume, mesh count should increase with $O(r^3)$.

Since number of unknowns is increasing computation time of the FMM code also increases. This is due to increased number of far field and near field interactions between the particles. While particle count increases, number of near field interactions increases with $O(N)$. However, far field interactions increases with $O(N^2)$ in single level FMM.

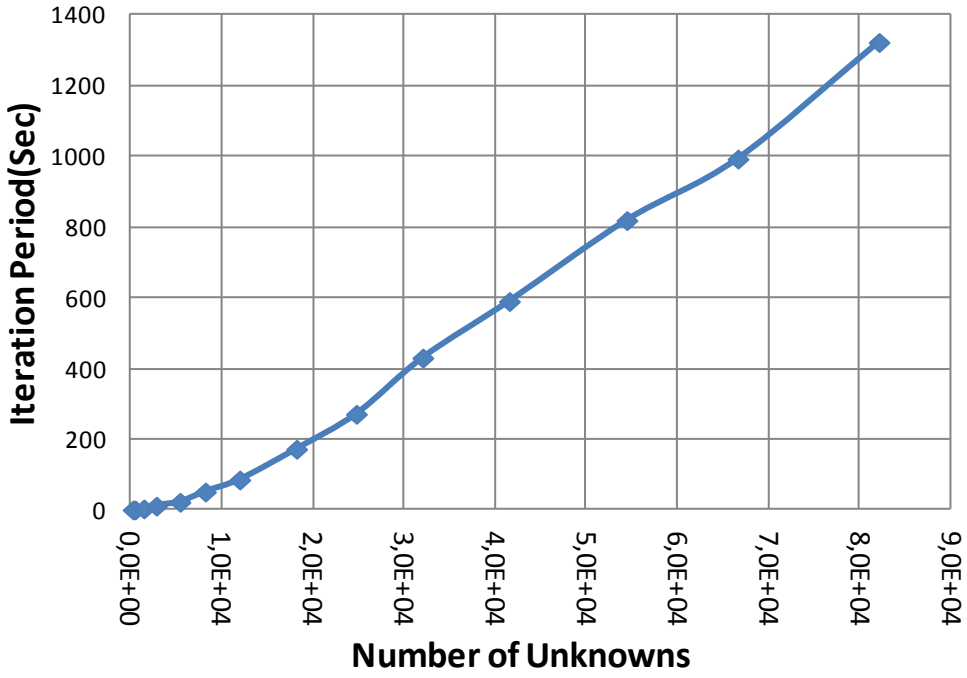

Figure 4.9 For various dielectric scatterer radius normalized monostatic RCS is calculated and compared with Mie series solution.

Basic assumption in O(N) and O(N^2) interaction count is that particle density is kept constant while meshing the object. Hence, due to constant particle density, near field interaction count will not increase with increased mesh size. Since, near field interactions are limited with a defined radius. Due to increased particle count, near field interactions increases linearly. However, this is not the case for far field interactions. Particles are distributed with a specific distance between each other. Hence, every group has approximately same number of scatterers. Hence, with increasing scatterer count, group count increases linearly. Due to interactions between the groups O(N^2) interactions has to be calculated. Hence, far field interactions in single level FMM is O(N^2). As can be seen from Figure 4.9, iteration time increases linearly with the number of unknowns. Therefore one can conclude that, for single iteration cycle, simulation time of the near field interactions dominates the simulation process. This is due to matrix-vector multiplications carried out with FMM operates faster than near field interactions. FMM operates on vectors and vector multiplications can be operated on groups of elements. However, for the

near interactions “for loops” in the program reduces the operation speed, since each element is operated sequentially. Due to random distribution of particles, near field interactions consume vast majority of the computation time. Actually, this is due to formulation of the problem. Since, dielectric body is finely meshed as closely fitted spheres; number of near interactions is considerably high. Since, computation space is dense; computation time that is spent on the near field interactions is several orders of magnitude higher than the time spent on the far field interactions in the electromagnetic solver.

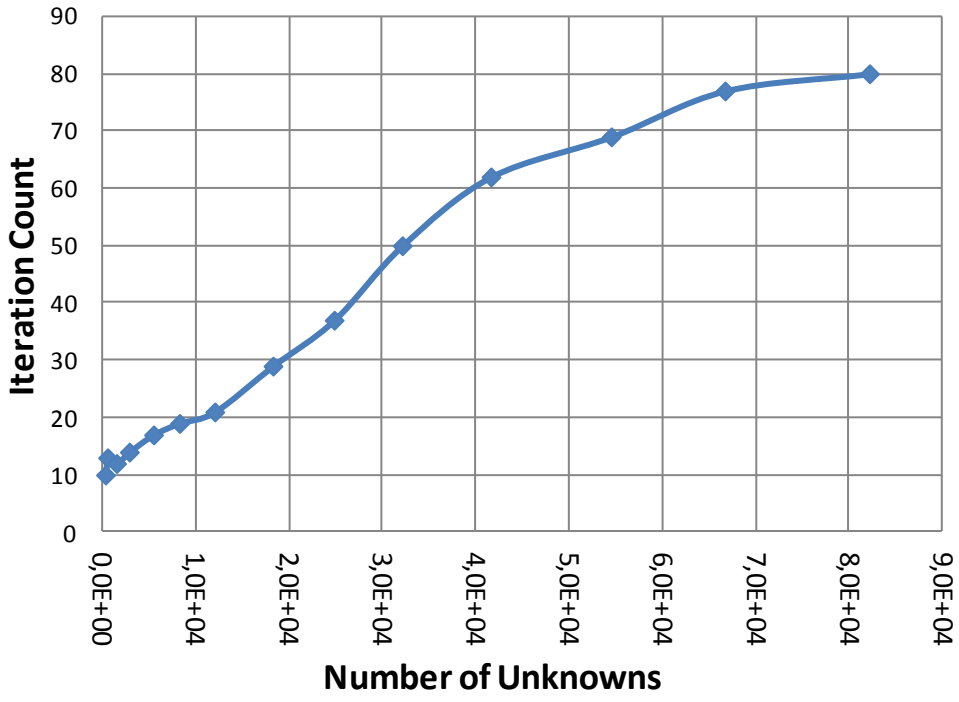

Figure 4.10 As the dielectric scatterer radius increases, number of unknowns also increases. Hence, with increased number of unknowns iteration count for required converge increases.

Total computation time depends on the iteration time, convergence rate of the iterative solver, and iteration count. With increased number of particles, iteration count increases. Increase in the iteration count with respect to increase in unknown number is given in Figure 4.10. As can be seen from the graph, as the dimension of the problem grows, iterative solver requires more steps in order to reach desired accuracy levels. For the dielectric scattering problem, solver converges with the desired accuracy as can be seen in Figure 4.13.

Due to the increased iteration count and longer iteration period, total simulation time increases with increased unknown count as expected. Total simulation time is given in Figure 4.11. Because of increased iteration count given in Figure 4.10 and increased simulation period given in Figure 4.9, total simulation time increases. Figure 4.11 demonstrates the total simulation time with varying number of unknowns.

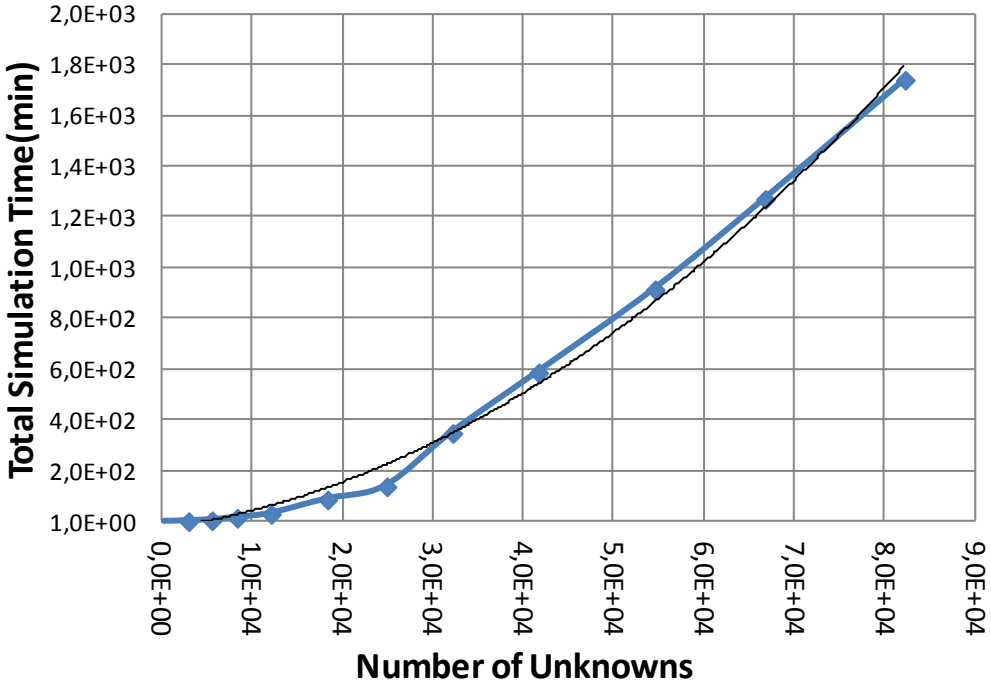

Figure 4.11 With increasing scatterer's radius, simulation time can be modeled as a second order polynomial. Simulation period is O(*N*) due to near field interactions. Iteration count also increases with *N*.

As can be seen from the Figure 4.11, computation time dependency is not linear as in the case of iteration period due to nonlinear increase in the iteration count. Hence iteration count is dependent on the dimension of the problem. Dependency of total computation time on number of unknowns can be modeled as a second order polynomial.

Memory used in the computations increases with increasing number of unknowns as can be seen in Figure 4.12. This is due to iterative methods used for

matrix inversion. Without the need of storing all matrix vector interactions, only vectors required for matrix multiplications are generated during the FMM process. Hence, instead of O(N^2) storage requirement, which is the case for direct solvers, iterative solvers requires O(N) memory allocation. Hence, using an ordinary personal computer, large electromagnetic problems can be attempted. All of the simulations given in this dissertation are performed on an Intel i5 M480 @2.67 GHz computer with 4GB of installed memory. Operation platform is Windows 7 Home Basic. Hence, using an ordinary computer, problems involving several hundred thousand unknowns can be solved.

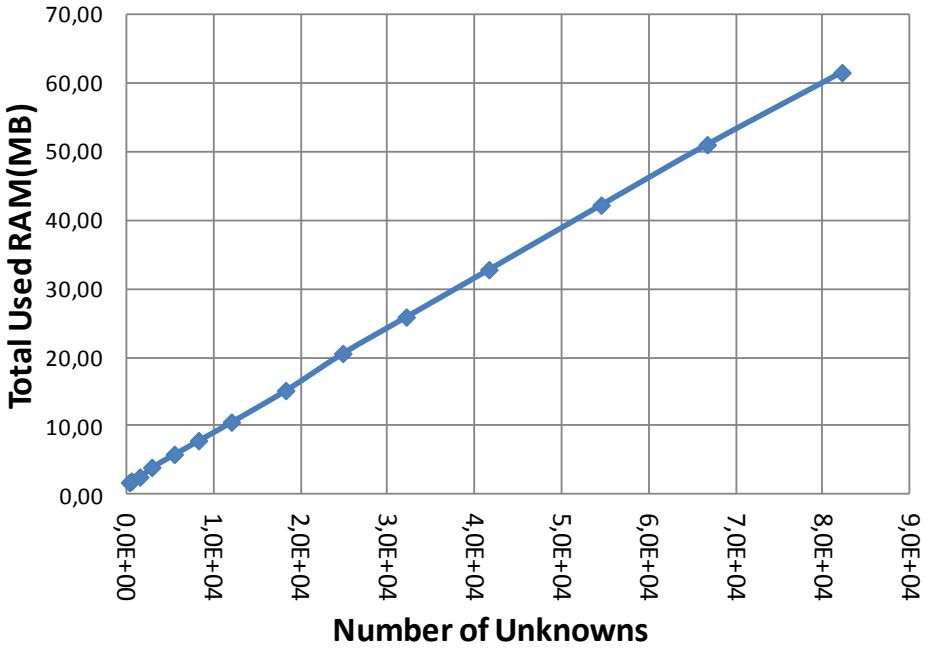

Figure 4.12 With increased number of unknowns, required memory size increases linearly. For direct solvers memory increases with O(N^2). Due to BiCGStab algorithm utilized, increase in memory is O(N).

In Figure 4.13 the convergence of iterative solver is given. The problem is the calculation of the RCS of a sphere located at the center of coordinate frame. Dielectric constant is 2.25 and radius is 0.75λ. The original problem is discretized as shown in Figure 4.6. Hence, results of the original problem and FMM solution can be compared. Total number of spheres used for representation of large sphere is 5137. Each sphere is described by 16 unknowns. Hence, total number of unknowns is

82192. Desired error threshold is set to be 1e-10. After 80 iteration steps error is reduced down to 5.6e-11, hence iteration stopped. Although desired accuracy is achieved, this error threshold is just for demonstration of the iterative solver. With increased iteration counts, error level can be further reduced. Error threshold can be determined according to the required accuracy of the computation and numerical precision used.

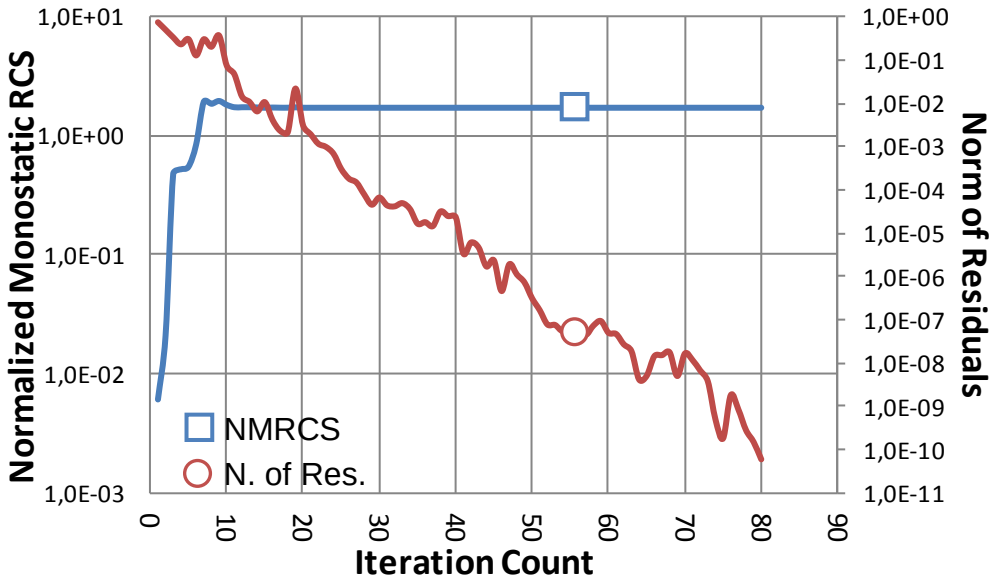

Figure 4.13 Simulation results of dielectric sphere with ε_r of 2.25 and radius of 0.75λ. Residual error gradually decreases below 1e-10 at 80th iteration. Normalized monostatic RCS of cluster of spheres are calculated as 1.7238. For residual errors below 1e-3, error in normalized monostatic RCS calculation is below 1%. Hence, 1e-3 can be used as an error threshold value.

As can be seen from Figure 4.13, reducing the error level down to 1e-10 is not necessary. At each iteration also normalized monostatic RCS of problem is calculated. Difference between the 1e-3 residual error and 1e-10 residual error is less than 1%. Hence error threshold can be increased to 1e-3 for this problem. Hence, simulation time can be improved by 75% for this particular case.

In Figure 4.14, residual errors for the dielectric spheres with 0.4λ, 0.5 λ, 0.6λ, and 0.75λ are demonstrated. Each problem is meshed with 0.07λ. Hence, Δm given

in equation (4-40) is selected as 0.07λ. Therefore, diameter of each small sphere is approximately 0.087λ. With this assumption, spheres are touching each other hence vector addition theorem is violated. However, as can be seen in Figure 4.14, convergence can be achieved despite of this violation. Also, as can be seen in Figure 4.7, simulation results are very close to the theoretical results. Hence, this violation does not pose a problem for dielectric scatterers with low dielectric constants. However, this is not the case for higher dielectric constants and metallic scatterers.

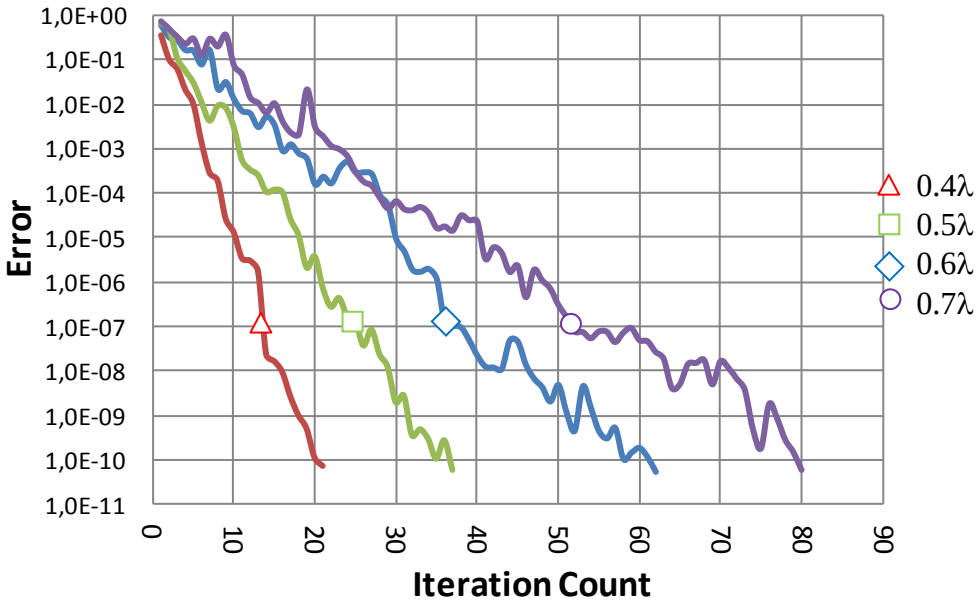

Figure 4.14 Residual error with respect to iteration count for various dielectric scatterers. With increasing diameter of scatterers, number of unknowns also increases. Hence, for higher number of unknowns, iteration count increases as well.

Performance parameters of the dielectric scattering problems are summarized in Table 4.1, Table 4.2, and Table 4.3. In each table, corresponding scatterer with radius identified in 'Dielectric size', is meshed with total number of '# of Particles' elements. For each mesh 16 unknowns are allocated and hence total unknown count is given by '# of Unknowns'. Peak memory requirement of the C++ code is provided in 'RAM' section.

As explained previously, iterative solvers generate a sequence that approximates to the solution of a linear system with reducing error at each successive

step. Hence, in order to reach an “acceptable” result, residual error of the solver should be below certain threshold provided by the programmer. Thus, instead of single solution cycle as in the case of direct solvers, convergence to solution is achieved in several steps. Hence, “Iteration Time” given in tables defines computation time of a single iteration. For a given error threshold of 1e-10, “Iteration Count” defines the required number of iteration in order to have error level less than given threshold. “Total Time” can be thought as multiplication of “Iteration Time” and “Iteration Count”. However, due to initial meshing steps and computation of translation coefficients, “Total Time” may differ slightly.

Table 4-1 Performance parameters for dielectric scattering problems for 0.1-0.3λ

Dielectric size(λ)	0,1	0,15	0,2	0,25	0,3
Iteration Time (sec)	0,3	0,38	3,2	11	22
Iteration Count	10	13	12	14	17
Total Time(min)	3,33E-02	8,33E-02	6,50E-01	2,65E+00	6,17E+00
RAM(MB)	1,80	2,00	2,60	4,00	5,90
# of Particles	19	33	93	179	341
# of Unknowns	3,0E+02	5,3E+02	1,5E+03	2,9E+03	5,5E+03

Table 4-2 Performance parameters for dielectric scattering problems for 0.35-0.55λ

Dielectric size(λ)	0,35	0,4	0,45	0,5	0,55
Iteration Time (sec)	51	85	172	271	430
Iteration Count	19	21	29	37	50
Total Time(min)	1,59E+01	3,12E+01	8,81E+01	1,40E+02	3,50E+02
RAM(MB)	7,90	10,60	15,20	20,60	25,90
# of Particles	515	751	1141	1551	2007
# of Unknowns	8,2E+03	1,2E+04	1,8E+04	2,5E+04	3,2E+04

Table 4-3 Performance parameters for dielectric scattering problems for 0.6-0.75λ

Dielectric size(λ)	0,6	0,65	0,7	0,75
Iteration Time (sec)	590	819	993	1323
Iteration Count	62	69	77	80
Total Time(min)	5,89E+02	9,16E+02	1,27E+03	1,74E+03
RAM(MB)	32,80	42,20	51,00	61,50
# of Particles	2601	3407	4169	5137
# of Unknowns	4,2E+04	5,5E+04	6,7E+04	8,2E+04

4.5.2 Scattering Calculations of NASA Almond

NASA almond as defined in [44], is commonly used as a benchmark tool for the evaluation and justification of computational electromagnetic solvers. Measurement and computation results at various frequencies of NASA almond are presented in the literature [45]. Since, scattering from a sphere is a very special case; RCS calculation of NASA almond is also considered in this study. Also, since scatterer is a metallic body, its effects on the convergence is investigated and RCS results are compared with measurements and other electromagnetic solvers.

Meshing of the NASA almond is provided in Figure 4.15 as cluster of spheres. Geometry of NASA almond is presented in [44]. According to boundaries of the NASA almond body, spheres with 0.04λ separation in space are filled throughout the body. Hence, instead of the actual structure, scattering problem from cluster of spheres is investigated at various frequencies.

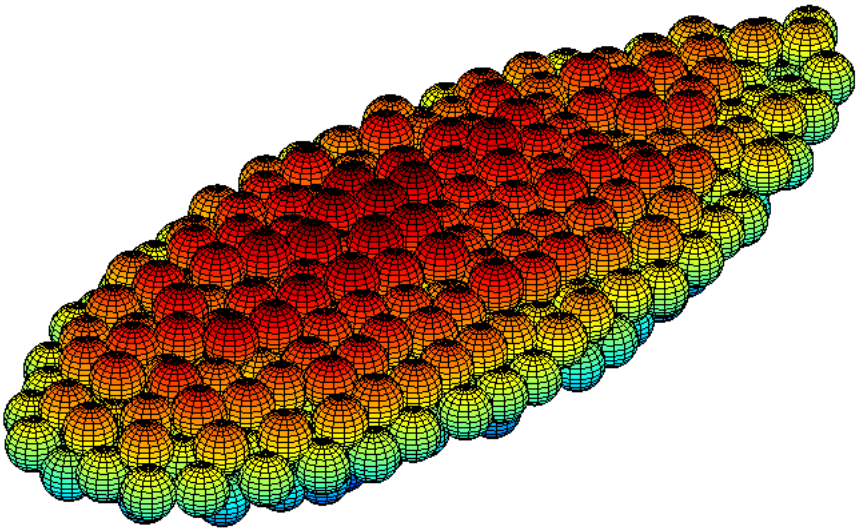

Figure 4.15 Mesh of NASA almond as a cluster of spheres at 1.19GHz is demonstrated. Center of the spheres are 0.04λ apart. Total number of spheres is 453. Monostatic RCS of the almond is simulated in VV and HH planes.

Mathematical description of NASA almond is provided in [44] as:

For $-0.41667 < t < 0$;

$$x=9.936.t$$

$$y=1.9209566\sqrt[2]{1-\left(\frac{t}{0.416667}\right)^2}\cos\phi \quad -\pi<\phi<\pi \tag{4-41}$$

$$z=0.6403156\sqrt[2]{1-\left(\frac{t}{0.416667}\right)^2}\sin\phi \quad -\pi<\phi<\pi$$

For $0 < t < 0.58333$;

$$x=9.936.t$$

$$y=48.02516\left[\sqrt[2]{1-\left(\frac{t}{2.08335}\right)^2}-0.96\right]\cos\phi \quad -\pi<\phi<\pi \tag{4-42}$$

$$z=16.00839\left[\sqrt[2]{1-\left(\frac{t}{2.08335}\right)^2}-0.96\right]\sin\phi \quad -\pi<\phi<\pi$$

Notice that coordinates generated with (4-41) and (4-42) are in inch scale.

Quality of the meshing and size of spheres plays crucial role in the accuracy of the computations. With selection of proper mesh size and sphere radius scattering

results provided in Figure 4.16 and Figure 4.17 are obtained. As can be inferred from the graphs, scattering problem can be approximated as distribution of spheres and calculation results are close to the original problem. For comparison, results of FEKO are also provided [45]. In Figure 4.16 and Figure 4.17, RCS calculations for horizontal and vertical polarizations are provided. Calculation performed in zero elevation and horizontal axis denotes ϕ variation. dBSM unit denotes dB with respect to one square meter. For all cases, monostatic RCS is calculated.

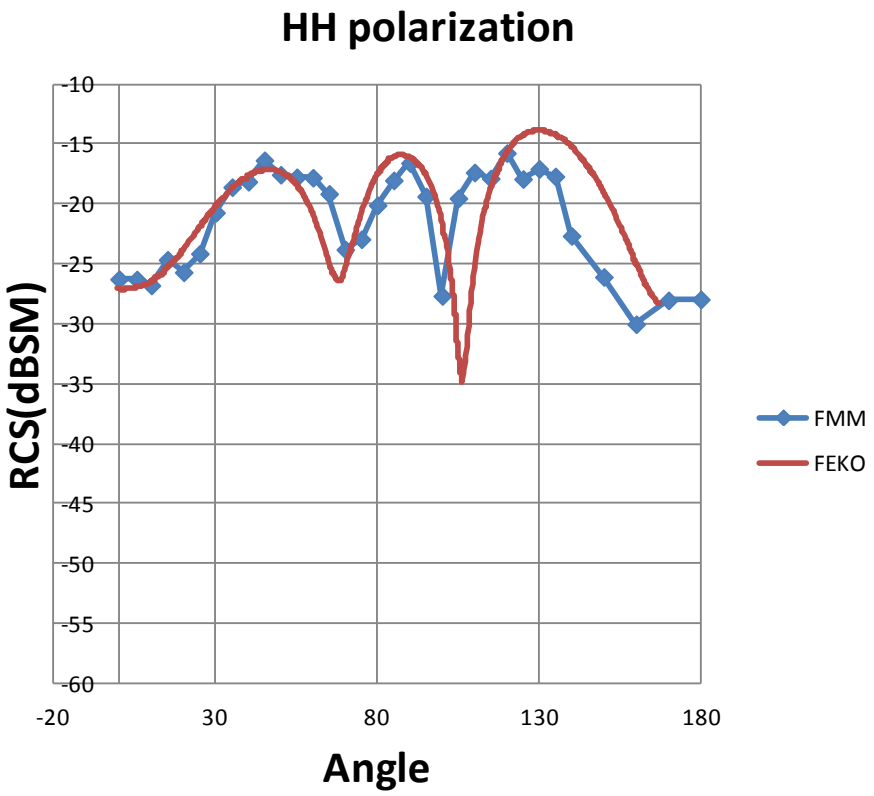

Figure 4.16 Comparison of the FMM simulations with the FEKO monostatic RCS for NASA almond at 1.19GHz. Minimum separation between the centers of the spheres is selected as 0.04λ . Radii of the spheres are 0.0232λ. Simulation result of horizontal polarization is provided.

With a variation on sphere radius and mesh size, results of the computations can drastically change. Using same mesh size with different sphere radius, vertical polarization results are provided in Figure 4.18. As can be seen from the graph, selection of the sphere radius as 0.02λ improves the vertical polarization solution of the scattering problem. However, horizontal polarization results differ from the

previous case. Solution of the horizontal polarization for a sphere radius of 0.02λ is given in Figure 4.19.

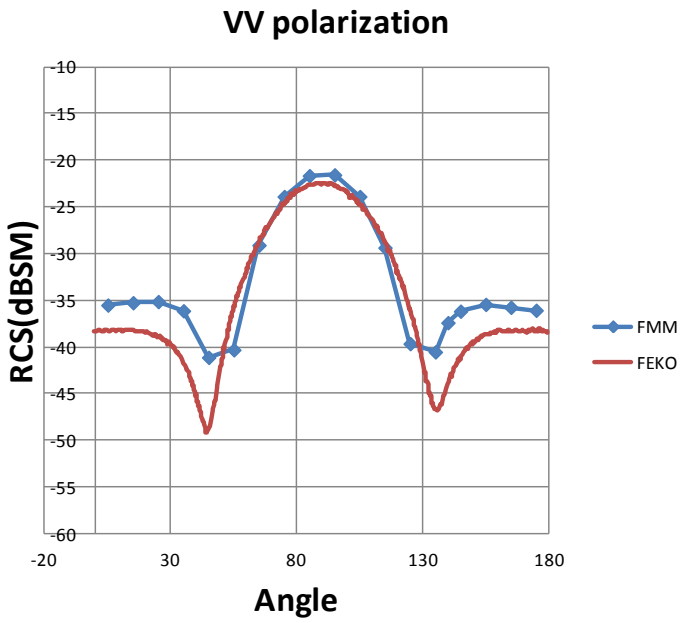

Figure 4.17 Comparison of the FMM simulations with the FEKO monostatic RCS for NASA almond at 1.19GHz. Minimum separation between the centers of the spheres is selected as 0.04λ . Radii of the spheres are 0.0232λ. Simulation result of vertical polarization is provided.

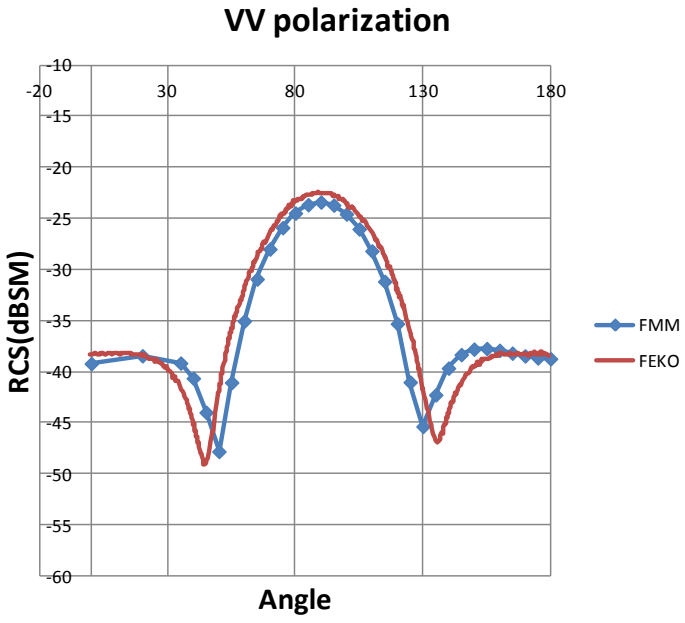

Figure 4.18 Comparison of the FMM simulations with the FEKO monostatic RCS for NASA almond at 1.19GHz. Minimum separation between the centers of the spheres is selected as 0.04λ . Radii of the spheres are 0.02λ. Simulation result of vertical polarization is provided.

As can be seen in Figure 4.19, results of FMM differ from FEKO results and the results obtained with 0.0232λ sphere radius shown in Figure 4.16. With reduced sphere size, convergence of the problem is improved since vector addition theorem is not violated. However, due to reduction of the sphere size, RCS of cluster of spheres is changed. Hence, selection of sphere radius as 0.02λ is not suitable for horizontal polarization.

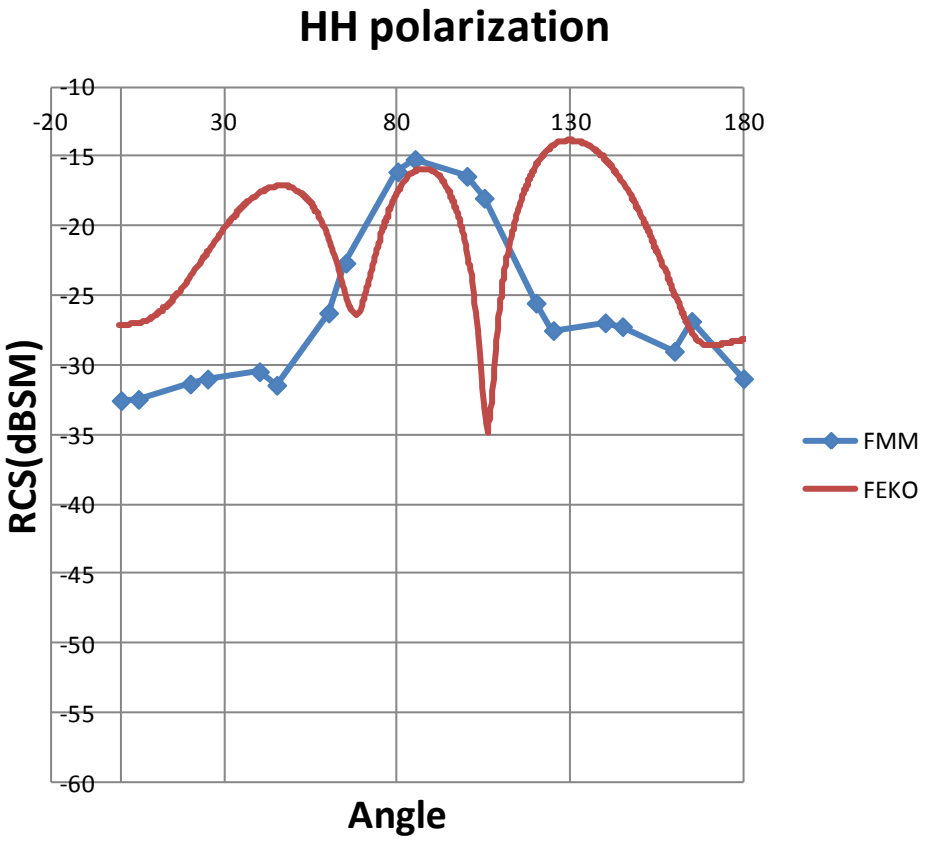

Figure 4.19 Comparison of the FMM simulations with the FEKO monostatic RCS for NASA almond at 1.19GHz. Minimum separation between the centers of the spheres is selected as 0.04λ . Radii of the spheres are 0.02λ. Simulation result of vertical polarization is provided.

NASA almond problem is attempted at various frequencies. Solution of problem at 1.19GHz is especially important due to wavelength of the solution

frequency is comparable with object dimensions. For 1.19GHz, length of the object is approximately equals to free space wavelength.

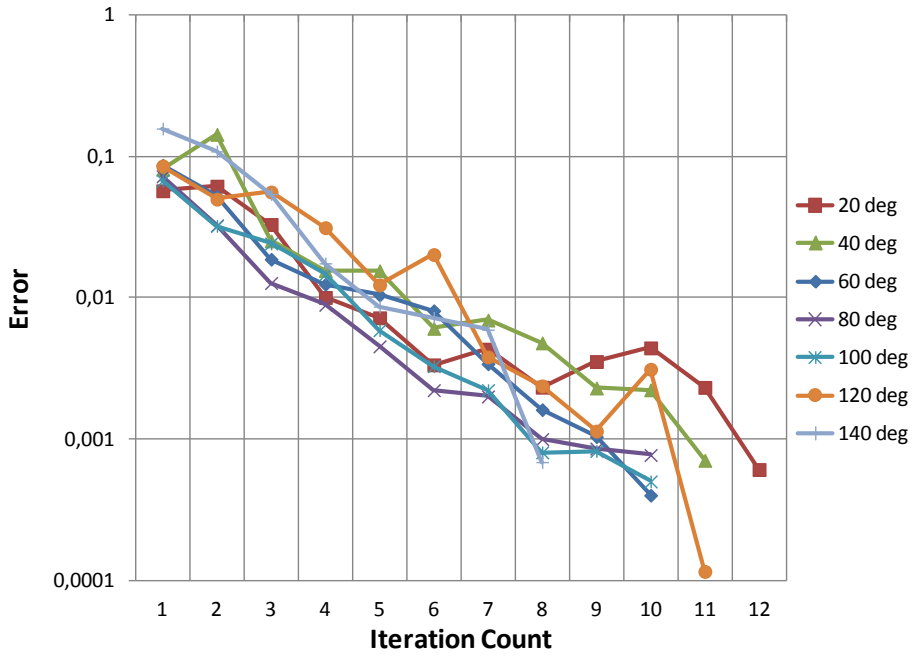

Figure 4.20 Convergence of the FMM results at various angles for monostatic RCS calculation of NASA almond at 1.19GHz. Minimum separation between the centers of the spheres is selected as 0.04λ . Radii of the spheres are 0.021λ. Simulation result of horizontal polarization is provided. (For clarity, only results of the selected angles are provided.)

Convergence of the scattering problem is also considered. As can be seen from the Figure 4.20, with a selection of sphere radius of 0.021λ, convergence with desired error threshold can be achieved in less than 12 iterations. Each iteration takes around 40 seconds with Intel i5 M480. Hence, total simulation time for an angle is around 8 minutes. Selection of sphere size plays important role on the convergence of the problem. With 0.02λ sphere size, convergence is fairly good. This corresponds to realistic problem where spheres are touching each other. Representation of mesh size and sphere radius is given in Figure 4.21. In order for vector addition theorem be applicable to scattering problem, spheres should not coincide with each other. Hence, mesh size should be larger than twice the sphere radius. For such a selection solver converges, however, as can be seen from the Figure 4.19, selection of sphere radius as half of the mesh size may not represent the electromagnetic scattering problem

adequately. Hence, sphere radius has to be increased, which causes convergence issues.

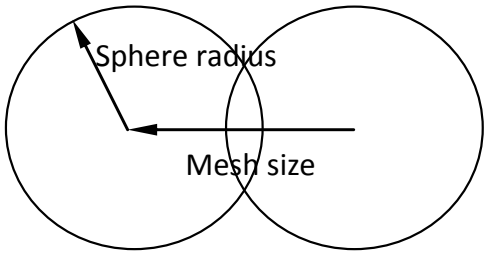

Figure 4.21 Demonstration of meshing of a volume using spheres. Selection of sphere radius as half of the mesh size or smaller corresponds to realistic problem. With selection of larger sphere size effects converge of the solver since model represents a fictitious problem.

At a higher frequency, same problem is addressed again. However, due to increased mesh count, instead of meshing whole almond body as in Figure 4.15, only surface of the almond is meshed. Hence a hollow structure shown in Figure 4.22 is obtained. By doing so, there is a considerable amount of saving in the particle count. Since scatterers are impenetrable, elements inside the volume should not contribute to the scattering problem. Therefore, hollow structure should provide similar results as meshing the whole body. Hence, instead of dealing with dense near field interactions among interior elements, which increase simulation time substantially, only interactions between the elements on the outer shell is computed, where interactions can be considered far.

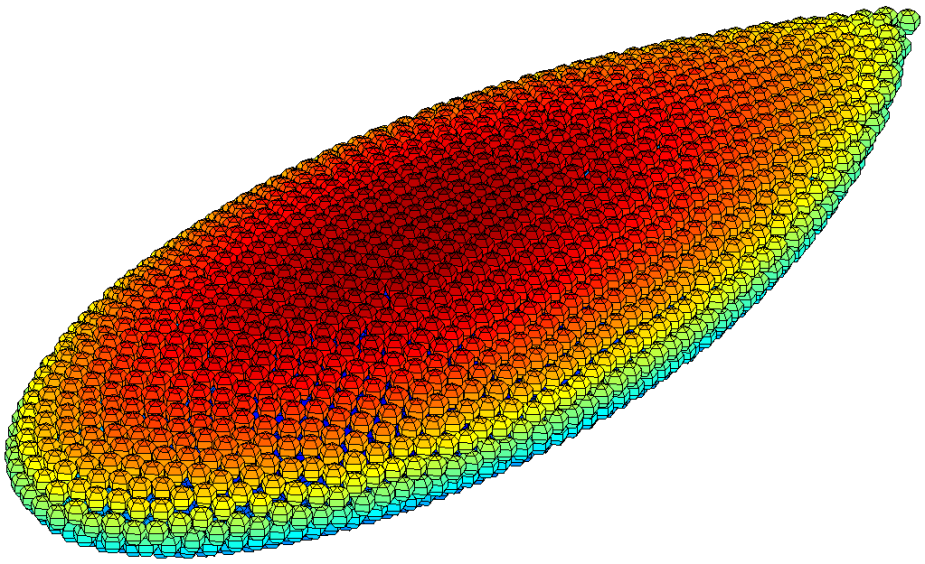

Figure 4.22 Mesh of NASA almond as a cluster of spheres at 7GHz is demonstrated. Center of the spheres are 0.1λ apart. Total number of spheres is 1995. Monostatic RCS of the almond is simulated in VV and HH planes.

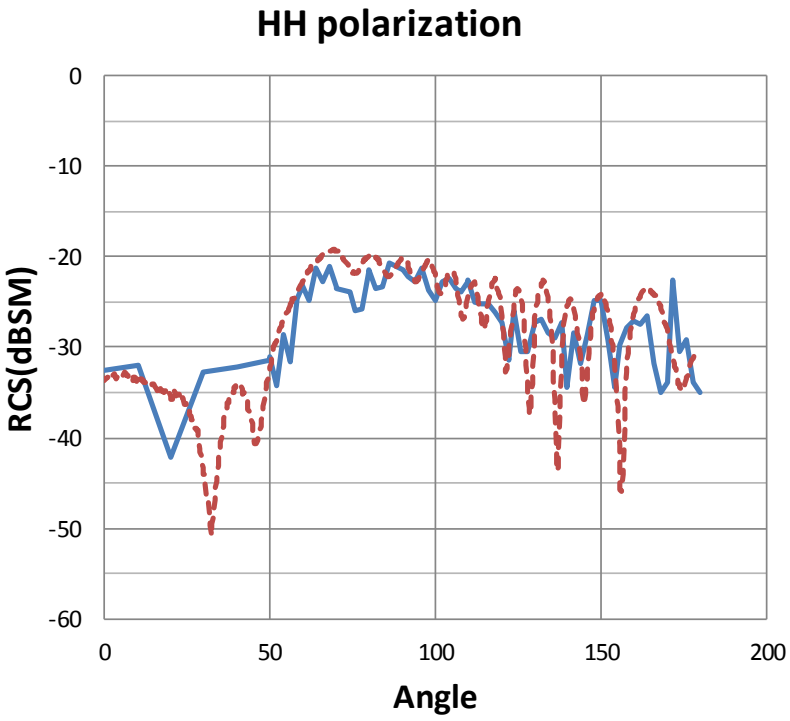

Figure 4.23 Comparison of the FMM simulations with the measurements of monostatic RCS for NASA almond at 7.0GHz. Minimum separation between the centers of the spheres is selected as 0.1λ. Radii of the spheres are 0.058λ. Simulation result of horizontal polarization is provided. Dashed line represents measurement result and solid line denotes FMM result.

As can be seen from Figure 4.23, there is a strong resemblance between the simulation results and measurements. Hence, with proper mesh size and modeling the shell of NASA almond as a cluster of spheres, electromagnetic scattering problem can be solved for horizontal polarization case. Total number of unknowns in this problem is 31920. Discrepancies between the results of the simulation and measurements should depend on the spherical modeling, since same problem is attempted with near field solver and results are very close to the FMM solutions.

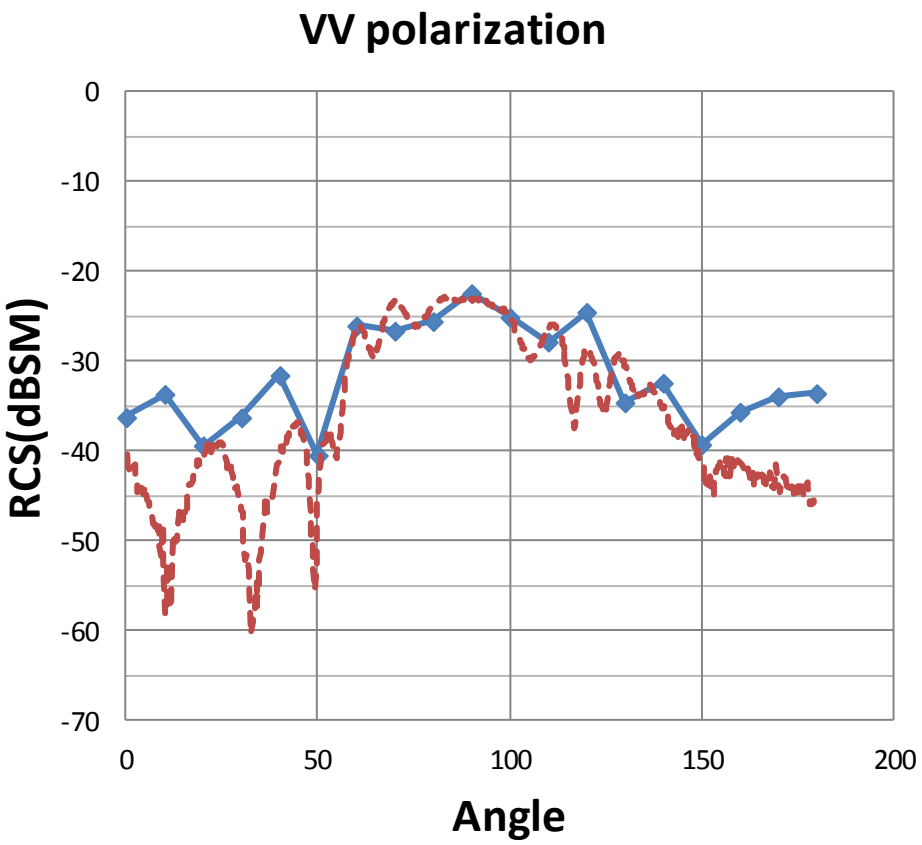

Figure 4.24 Comparison of the FMM simulations with the measurements of monostatic RCS for NASA almond at 7.0GHz. Minimum separation between the centers of the spheres is selected as 0.1λ. Radii of the spheres are 0.058λ. Simulation result of vertical polarization is provided. Dashed line represents measurement result and solid line denotes FMM result.

Again simulation results for the vertical polarization and measurement results are correlated as can be seen from Figure 4.24. Hence, meshing used for horizontal polarization is also applicable to the vertical polarization.

Simulation frequency is further increased to 9.92 GHz and calculations are performed. As in the case of Figure 4.22, only the surface of the NASA almond is meshed in order to reduce mesh count and decrease near field interactions. Mesh size is selected as 0.1λ and radius of spheres is selected as 0.058λ. Resultant mesh is similar to the previous mesh structure given in Figure 4.22 and will not be repeated here. Vertical and horizontal polarization results are compared with the measurement results and are given in Figure 4.25 and Figure 4.26.

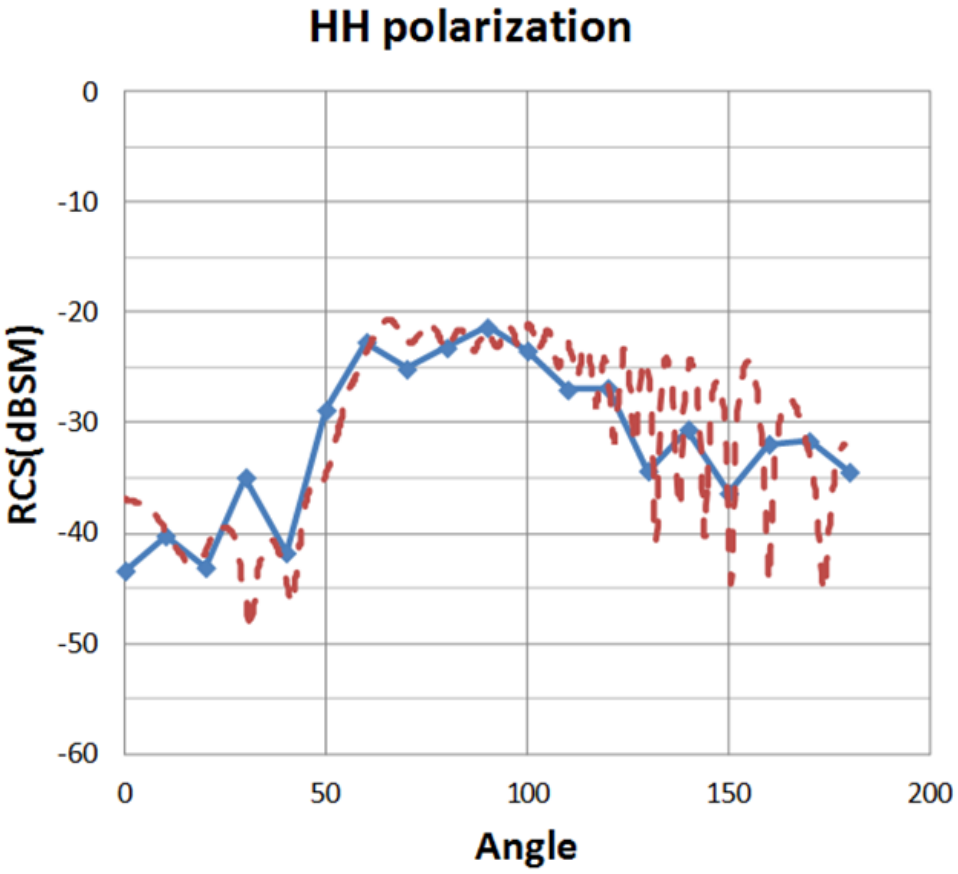

Figure 4.25 Comparison of the FMM simulations with the measurements of monostatic RCS for NASA almond at 9.92GHz. Minimum separation between the centers of the spheres is selected as 0.1λ . Radii of the spheres are 0.058λ. Simulation result of horizontal polarization is provided. Dashed line represents measurement result and solid line denotes FMM results [45].

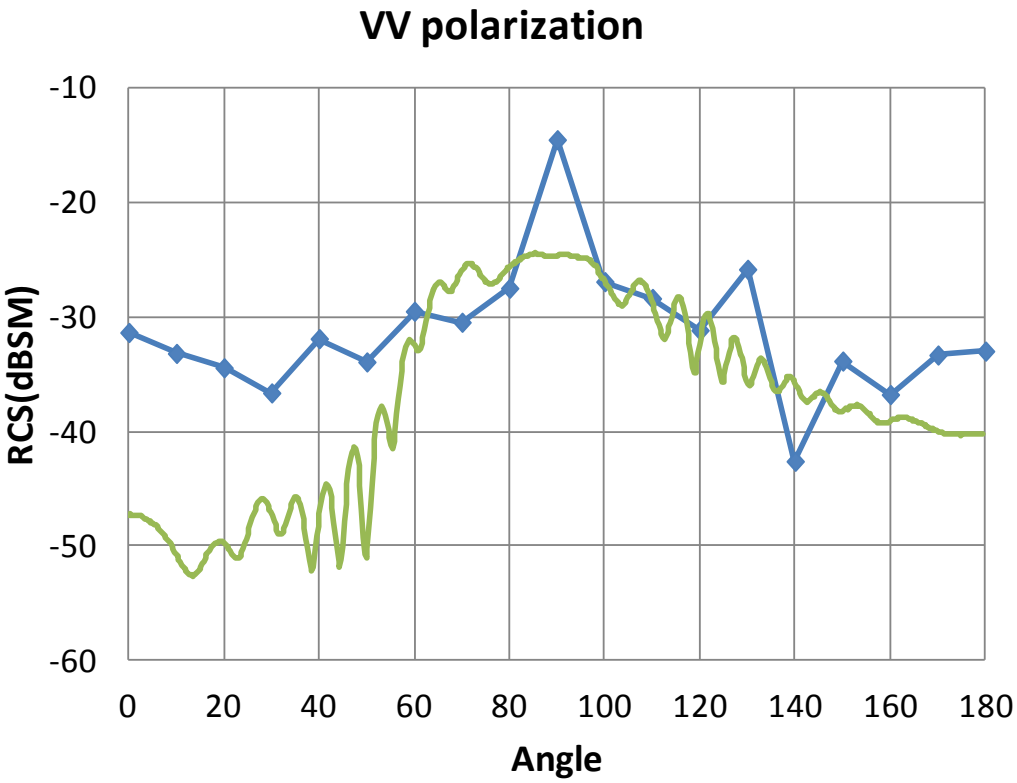

Figure 4.26 Comparison of the FMM simulations with the FEKO simulations of monostatic RCS for NASA almond at 9.92GHz. Minimum separation between the centers of the spheres is selected as 0.1λ . Radii of the spheres are 0.058λ. Simulation result of vertical polarization is provided. Line with diamond marker is FMM results.

As can be seen from the graphs given in Figure 4.25 and Figure 4.26, there is a general agreement with computation and measurement results.

CHAPTER 5

CONCLUSIONS

Contribution of this thesis is the implementation of diagonalization of the vector addition theorem introduced by Chew [35] for the solution of electromagnetic scattering problems composed of randomly distributed spheres.

For the solution of generic scattering problems, several fundamental theorems were investigated. In order to take advantage of spherical symmetry, vector spherical wave functions were reviewed. Scalar and vector addition theorems were examined for the translation of the field from source to scatterer coordinates. Also, plane waves were expanded in terms of vector spherical wave functions, in order to define incoming fields onto the scatterers due to external sources. T-matrix formulation was examined for the solution of scattering from single particle problem. With increased particle count direct implementation of the particle interactions were found to be inefficient due to increased number of matrix vector multiplications. Hence, vector addition theorems were diagonalized to reduce far field interactions.

FMM solver was implemented to solve multiple scattering problems for arbitrary distribution of spheres. Using FMM solver, scattering from dielectric and metallic test bodies were investigated. Since solver relies on T-matrix formulation, instead of computation of isolated T-matrices, objects were transformed to smaller bodies where T-matrices were known or easily computable. Due to the orthogonality of the vector spherical wave functions on spherical coordinates, boundary conditions were easily applied and T-matrix could be formed for a spherical scatterer. Since, T-matrix of a sphere is readily available, it is useful to represent scattering bodies of arbitrary shape by a cluster of small spheres. Then, scattering problem for cluster of spheres was investigated using FMM. Due to increased number of unknowns instead of direct solvers, iterative solvers are used. Iterative solvers provide better

performance in terms of memory allocation and solution speed of matrix equations. Using the analyzed algorithms, an electromagnetic solver is implemented using C++. Developed tool is tested for convergence, memory allocation and accuracy using a number of test bodies. Scattering problems involving more than 380000 unknowns are numerically solved with developed tool. For the solution of the problems an ordinary PC was used, since memory requirements for the given problem was just 280MB. Finally, monostatic RCS results obtained by FMM are compared with the measurement results of the dielectric sphere and metallic NASA almond.

REFERENCES

[1] Y. Chu, "Fast Algorithm for Electrically Small Inhomogeneous Medium Structures," Ph.D. dissertation, Elect. Eng., Univ. Illinois, Urbana-Champaign, 2004.

[2] J. M. Jin, "*The Finite Element Method in Electromagnetics*," New York: John Wiley & Sons, 2001.

[3] K. S. Yee, "Numerical Solutions of Initial Boundary Value Problems Involving Maxwell's Equations in Isotropic Media," *IEEE Transactions Antennas Propagat*., vol. 14, pp. 302-307, May 1966.

[4] A. F. Peterson, "Analysis of heterogeneous electromagnetic scatterers: Research progress of the past decade," *Proceedings IEEE*, vol. 79, no. 10, pp. 1431-1441. Oct. 1991.

[5] D. E. Livesay and K. Chen, "Electromagnetic fields induced inside arbitrarily shaped biological bodies," *IEEE Transactions Microwave Theory Tech*., vol. 22, pp. 1273-1280, Dec. 1974.

[6] D. H. Schaubert, D. R. Wilton, and A. W. Glisson, "A tetrahedral modeling method for electromagnetic scattering by arbitrarily shaped inhomogeneous dielectric bodies," *IEEE Transactions Antennas Propaqat*., vol. 32, pp. 77-85, Jan. 1984.

[7] R. New and T. J. Eisler, "Acoustic radiation from multiple spheres," *J. Sound Vib.* 22, pp. 1-17, 1972.

[8] C. Liang and Y. T. Lo, "Scattering by two spheres," *Radio Sci*. 2, pp. 1481-1495, 1967.

[9] J. H. Bruning and Y. T. Lo, "Multiple scattering of EM waves by spheres. Part I— Multipole expansion and ray-optical solutions," *IEEE Trans. Antennas Propag.* AP-19, pp. 378-390, 1971.

[10] J. H. Bruning and Y. T. Lo, "Multiple scattering of EM waves by spheres. Part II— Numerical and experimental results," *IEEE Trans. Antennas Propag*. AP-19, pp. 391-400, 1971.

[11] A-K. Hamid, I. R. Ciric, and M. Hamid, "Multiple scattering by a linear array of conducting spheres," *Can. J. Phys*. 68, pp. 1157-1168, 1990.

[12] A-K. Hamid, I. R. Ciric, and M. Hamid, "Electromagnetic scattering by an arbitrary configuration of dielectric spheres," *Can. J. Phys*. 68, pp. 1419-1428, 1990.

[13] A-K. Hamid, I. R. Ciric, and M. Hamid, "Iterative solution of the scattering by an arbitrary configuration of conducting or dielectric spheres," *IEE Proceedings-H* 138, pp. 565-572, 1991.

[14] D. W. Mackowski, "Analysis of radiative scattering for multiple sphere configurations," *Proc. R. Soc. Lond*. A 433, pp. 599-614,1991.

[15] F. de Daran, V. Vigneras-Lefebvre, and J. P. Pameix, "Modeling of electromagnetic waves scattered by a system of spherical particles," *IEEE Trans. Magn*. 31, pp. 1598-1600, 1995.

[16] F. Borghese, P. Denti, R. Saija, G. Toscano, and O. I. Sindoni, "Effects of aggregation on the electromagnetic resonance scattering of dielectric spherical objects," *Nuovo Cimento D 6D*, pp. 545-558, 1985.

[17] F. Borghese, P. Denti, R. Saija, G. Toscano, and O. I. Sindoni, " Multiple electromagnetic scattering from a cluster of spheres. I. Theory," *Aerosol Sci. Tech*. 3, pp. 227-235,1984.

[18] F. Borghese, P. Denti, G. Toscano, and O. I. Sindoni, "Electromagnetic scattering by a cluster of spheres," *Appl. Opt.* 18, pp. 116-120, 1979.

[19] O. I. Sindoni, F. Borghese, P. Denti, R. Saija, and G. Toscano, "Multiple electromagnetic scattering from a cluster of spheres. II. Symmetrization," *Aerosol Sci. Tech.* 3, pp. 237-243, 1984.

[20] M. Quinten and U. Kreibig, "Absorption and elastic scattering of light by particle aggregates," *Appl. Opt.* 32, pp. 6173-6182, 1993.

[21] P. C. Waterman, "New formulation of acoustic scattering," *J. Acoust. Soc. Am*. 45, pp. 1417-1429, 1969.

[22] P. C. Waterman, "Symmetry, unitarity, and geometry in electromagnetic scattering," *Phys. Rev*. D 3, pp. 825-839, 1971.

[23] P. C. Waterman, "Matrix theory of elastic wave scattering," *J. Acoust. Soc. Am.* 60, pp. 567-580, 1976.

[24] P. C. Waterman, "Matrix theory of elastic wave scattering. II. A new conservation law," *J. Acoust. Soc. Am*. 63, pp. 1320-1325, 1978.

[25] Greengard, and V. Rokhlin "A fast algorithm for particle simulations," *Journal of Computational Physics*, 1987.

[26] Barry A. Cipra, "The best of the 20th century: editors name top 10 algorithms," *SIAM news* 33.4 1-2, 2000.

[27] S. Koc and W. C. Chew, "Calculation of acoustical scattering from a cluster of scatterers." *The Journal of the Acoustical Society of America* 103.2 pp.721-734, 1998.

[28] Weng Cho Chew and Y. M. Wang. "Efficient ways to compute the vector addition theorem," *Journal of electromagnetic waves and applications* 7.5, pp. 651-665, 1993.

[29] J. Richie, (2011, June), *Vector Spherical Wave Functions: Library and Test Codes* [online]. Available: http://www.eng.mu.edu/~richiej/seminar/vswf.pdf

[30] W.C. Chew, "Integral Equations," in *Waves and Fields in Inhomogeneous Media*, 1st ed. New York: IEEE Press Series on Electromagnetic Waves,1990,ch 8, pp 429-443.

[31] J. A. Stratton, "Boundary-Value Problems", in *Electromagnetic Theory*, 1st ed. New York and London: McGraw-Hill Book Company, 1941, ch. 9, sec. 8, pp 563-573.

[32] Yousef Saad, "Krylov Subspace Methods-Part II", in *Iterative methods for sparse linear systems*. 2nd ed. Siam 2003, ch. 7, sec. 3, pp 211-212.

[33] Y. Saad and M. H. Schultz. "GMRES: a generalized minimal residual algorithm for solving nonsymmetric linear systems". *SIAM Journal on Scientic and Statistical Computing*, 7:856-869, 1986.

[34] Nail A. Gumerov and Ramani Duraiswami, "Computation of scattering from clusters of spheres using the fast multipole method." *The Journal of the Acoustical Society of America* 117.4 (2005): 1744-1761.

[35] W. C. Chew, "Vector Addition Theorem and Its Diagonalization," *Communications in Computational Physics*, Vol. 3, No. 2, pp. 330-341.

[36] D. W. Mackowski, "Calculation of total cross sections of multiple-sphere clusters." *JOSA A* 11.11 (1994): 2851-2861.

[37] Eibert, Thomas F. "A diagonalized multilevel fast multipole method with spherical harmonics expansion of the k-space integrals," *Antennas and Propagation, IEEE Transactions* on 53.2 (2005): 814-817.

[38] W. C. Chew, S. Koc, J. Song, L. Lu, E. Michielssen, "A Succint Way to Diagonalize the Translation Matrix in Three Dimensions" *Microwave and Optical Technology Letters*, 15 , (1997), p.144-147.

[39] W. C. Chew, J. M. Jin, E. Michielssen, J. Song, "Fast Multipole Method and Multilevel Fast Multipole Algorithm in 2D", in *Fast and Efficient Algorithms in Computational Electromagnetcis*. 1st ed. Boston and London: Artech House Publishers, 2001, ch. 2, sec. 2, pp 52-53.

[40] E.Darve "The Fast Multipole Method I:Error Analysis and Asymptotic Complexity" *SIAMJ. Numer Anal*., Vol 38, No 1, pp98-128.

[41] S. Koc, Sencer, Jiming Song, and Weng Cho Chew. "Error analysis for the numerical evaluation of the diagonal forms of the scalar spherical addition theorem." *SIAM Journal on Numerical Analysis* 36.3 (1999): 906-921.

[42] Li Jun Jiang and Weng Cho Chew. "A mixed-form fast multipole algorithm." *Antennas and Propagation, IEEE Transactions* on 53.12 (2005): 4145-4156.

[43] C. Balanis "Scattering", in *Advanced Engineering Electromagnetics*. 1st ed. New Jersey: John Wiley & Sons, 1989, ch. 11, sec. 7, pp 650-658.

[44] C. Woo, H. T. Wang, M. J. Schuh, and M. L. Sanders, "EM programmer's notebook-benchmark radar targets for the validation of computational electromagnetics programs." *Antennas and Propagation Magazine, IEEE* 35.1 (1993): 84-89.

[45] FEKO(2013, May)[online]. Available, http://www.emssusa.com/emssusa/Products/Application_Notes/FEKOUtilities//FEKOApplicationNotes_RCS.pdf

[46] W. C. Chew, *"*Diagonalization of the Vector Addition Theorem,*" IEEE Antennas and Propagation Society International Symposium* 2007,pp3440-3443.

[47] W. C. Chew, J. M. Jin, E. Michielssen and J. M. Song, *"Fast and Efficient Algorithms in Computational Electromagnetics"*, Boston, MA: Artech House, 2001.

[48] W.C. Chew, "Recurrence Relations for Three-Dimensional Scalar Addition Theorem", *Journal of Electromagnetic Waves and Applications*, 6.1-4 (1992), pp. 133-142.

[49] R. Coifman, V. Rokhlin, S. Wandzura "The Fast Multipole Method for the Wave Equation: A Pedestrian Prescription" Antennas and Propagation Magazine, IEEE 35.3 (1993): pp. 7-12.

[50] S. Sencer Koc. EE521. Class Lecture, Topic: "Scattering From a Perfectly Conducting Sphere" Middle East Technical University, Ankara, Turkey, Sept,2008.

[51] Epton, Dembart “Multipole Translation Theory for Three Dimensional Laplace and Helmholtz Equations” *SIAM Journal on Scientific Computing* 16.4 (1995), pp. 865-897

[52] E. Darrigrand “Coupling of Fast Multipole Method and Microlocal Discretization for the 3-D Helmholtz Equation” Journal of Computational Physics Vol 181, Issue 1, 2002, pp 126-154.

[53] N. A. Gumerov, R. Duraiswami “Fast Multipole Method for the Helmholtz Equation in Three Dimensions” Ed. 1, I. Mayergoyz, Amsterdam:Elsevier Series in Electromagnetism, 2004.

[54] Chew, Lu, Wang “Efficient Computation of Three-Dimensional Scattering of Vector Electromagnetic Waves” JOSA A, 1994, pp. 1528-1537.

[55] Jiming Song, Cai-Cheng Lu, and Weng Cho Chew. "Multilevel fast multipole algorithm for electromagnetic scattering by large complex objects." *Antennas and Propagation, IEEE Transactions on* 45.10 ,1997, pp.1488-1493.

[56] Weng Cho Chew et al. "Fast solution methods in electromagnetics."*Antennas and Propagation, IEEE Transactions on* 45.3,1997, pp. 533-543.

[57] Robert L Wagner and Weng Cho Chew. "A ray-propagation fast multipole algorithm." *Microwave and Optical Technology Letters* 7.10, 1994, pp. 435-438.

[58] J. M. Song and Weng Cho Chew. "Multilevel fast-multipole algorithm for solving combined field integral equations of electromagnetic scattering."*Microwave and Optical Technology Letters* 10.1, 1995, pp. 14-19.

[59] Eric Darve and Pascal Havé. "Efficient fast multipole method for low-frequency scattering." *Journal of Computational Physics* 197.1, 2004, pp. 341-363.

[60] Eric Darve. "The fast multipole method: numerical implementation." *Journal of Computational Physics* 160.1, 2000, pp. 195-240.

[61] Y. J, Liu and N. Nishimura. "The fast multipole boundary element method for potential problems: a tutorial." *Engineering Analysis with Boundary Elements* 30.5, 2006, pp. 371-381.

[62] Vikas Chandrakant Raykar. "A short primer on the fast multipole method." http://www.umiacs.umd.edu/labs/cvl/pirl/vikas/publications/FMM_tutorial.pdf, 08.2013.

[63] George Collins. (2003) Fundamental numerical methods and data analysis." (Ed. 2). [On-line]. Available: http://ads.harvard.edu/books/1990fnmd.book/

[64] V. Rokhlin. "Diagonal forms of translation operators for the Helmholtz equation in three dimensions." *Applied and Computational Harmonic Analysis1.1*, 1993,pp. 82-93.

[65] Jian-Ying Li, and Le-Wei Li. "Characterizing scattering by 3D arbitrarily shaped homogeneous dielectric objects using fast multipole method." *Antennas and Wireless Propagation Letters, IEEE* 3.1, 2004 ,pp. 1-4.

[66] Chunlei Guo, and Todd H. Hubing. "Development and application of a fast multipole method in a hybrid FEM/MoM field solver." *ACES*. Vol. 19. No. 3. 2004.

[67] Frank Ethridge, and Leslie Greengard. "A new fast-multipole accelerated Poisson solver in two dimensions." *SIAM Journal on Scientific Computing* 23.3, 2001, pp.741-760.

[68] Rick Beatson, and Leslie Greengard. "A short course on fast multipole methods." *Wavelets, multilevel methods and elliptic PDEs*, 1997, pp. 1-37.

[69] Vladimir Rokhlin,. "Rapid solution of integral equations of scattering theory in two dimensions." *Journal of Computational Physics* 86.2, 1990, pp. 414-439.

[70] Leslie, Greengard, and Vladimir Rokhlin. "A new version of the fast multipole method for the Laplace equation in three dimensions." *Acta numerica* 6.1, 1997, pp. 229-269.

[71] J. M. Song, , and W. C. Chew. "Fast multipole method solution of three dimensional integral equation." *Antennas and Propagation Society International Symposium. AP-S. Digest*. Vol. 3. IEEE, 1995.

[72] Ben Dembart, and Elizabeth Yip. "The accuracy of fast multipole methods for Maxwell's equations." *Computational Science & Engineering, IEEE* 5.3, 1998, pp. 48-56.

[73] Song, J. M., and Weng Cho Chew. "Multilevel fast-multipole algorithm for solving combined field integral equations of electromagnetic scattering."*Microwave and Optical Technology Letters* 10.1, 1995, pp. 14-19.

[74] Gumerov, Nail A., and Ramani Duraiswami. (2001) "Fast, exact, and stable computation of multipole translation and rotation coefficients for the 3-D helmholtz equation." Available: http://drum.lib.umd.edu/bitstream/1903/1141/1/CS-TR-4264.pdf [11.2014].

[75] W. L.Moreira et al. "Expansion of arbitrary electromagnetic fields in terms of vector spherical wave functions." *arXiv preprint arXiv:1003.2392*, 2010.

[76] Felderhof, B. U., and R. B. Jones. "Addition theorems for spherical wave solutions of the vector Helmholtz equation." *Journal of Mathematical Physics* 28, 1987, pp. 836.

[77] Friedman, Bernard, and Joy Russek. "Addition theorems for spherical waves."*Quart. Appl. Math* 12.13, 1954.

[78] Bohren, Craig F., and Donald R. Huffman. "Absorption and scattering by a sphere." *Absorption and Scattering of Light by Small Particles*, 1983, pp. 82-129.

[79] Lu, Cai-Cheng, and Weng Cho Chew. "Fast far-field approximation for calculating the RCS of large objects." *Microwave and Optical Technology Letters* 8.5, 1995, pp. 238-241.

[80] Boström, Anders, Gerhard Kristensson, and Staffan Ström. "Transformation properties of plane, spherical and cylindrical scalar and vector wave functions."*Acoustic, Electromagnetic and Elastic Wave Scattering, Field Representations and Introduction to Scattering* 1, 1991, pp. 165-210.

[81] Cheng, Hongwei, Leslie Greengard, and Vladimir Rokhlin. "A fast adaptive multipole algorithm in three dimensions." *Journal of Computational Physics*155.2, 1999, pp. 468-498.

[82] Cao, P., and C. Macaskill. "Iterative techniques for rough surface scattering problems." *Wave Motion* 21.3, 1995, pp. 209-229.

[83] Gumerov, Nail A., and Ramani Duraiswami. "Computation of scattering from N spheres using multipole reexpansion." *The Journal of the Acoustical Society of America* 112, 2002, pg 2688.

[84] Lin, J. H., and W. C. Chew. "BiCG-FFT T-Matrix method for solving for the scattering solution from inhomogeneous bodies." *Microwave Theory and Techniques, IEEE Transactions on* 44.7,1996 , pp 1150-1155.

[85] Lu, CaiCheng, and Weng Chup Chew. "Fast algorithm for solving hybrid integral equations." *IEE Proceedings H (Microwaves, Antennas and Propagation)*. Vol. 140. No. 6. IET Digital Library, 1993.

[86] Hastriter, Michael Larkin, Shinichiro Ohnuki, and Weng Cho Chew. "Error control of the translation operator in 3D MLFMA." *Microwave and Optical Technology Letters* 37.3, 2003, pp. 184-188.

[87] Wang, Z. L., L. Hu, and W. G. Lin. "Modified T-matrix formulation for multiple scattering of acoustic waves." *Waves in random media* 4.3, 1994.

[88] Stein, Seymour. "Addition theorems for spherical wave functions." *Quart. Appl. Math.* 19, 1961, pp. 15-24.

[89] Orval R. Cruzan,. "Translational addition theorems for spherical vector wave functions." *Q. Appl. Math* 20.1, 1962, pp. 33-40.

[90] Dufva, Tommi J., Jukka Sarvas, and Johan C-E. Sten. "Unified derivation of the translational addition theorems for the spherical scalar and vector wave functions." *Progress In Electromagnetics Research B* 4, 2008, pp. 79-99.

[91] Chew, Weng C. "A derivation of the vector addition theorem." *Microwave and Optical Technology Letters* 3.7, 1990, pp. 256-260.

CURRICULUM VITAE

PERSONAL INFORMATION

Surname, Name: Atasoy, Halil İbrahim
Nationality: Turkish (TC)
Date and Place of Birth: 15 April 1983 , Ankara
Marital Status: Married
Phone: +90 312 592 35 64
email: hibrahimatasoy(at)hotmail(dot)com

EDUCATION

Degree	Institution	Year of Graduation
MS	METU Electrical and Electronics Engineering	2007
BS	METU Electrical and Electronics Engineering	2005

WORK EXPERIENCE

Year	Place	Enrollment
2009- Present	ASELSAN A.Ş.	Microwave Design Engineer
2005-2009	METU Department of Electrical and Electronics Engineering	Researcher

FOREIGN LANGUAGES

Advanced English, Basic German